THE ASTROPHYSICAL JOURNAL, 393:307–328, 1992 July 1

SPHERICALLY SYMMETRIC, EXPANDING, NON–LTE MODEL ATMOSPHERES FOR NOVAE DURING THEIR EARLY STAGES

P. H. HAUSCHILDT[1] AND R. WEHRSE
Institut für Theoretische Astrophysik, D-6900 Heidelberg, Germany

S. STARRFIELD
Department of Physics and Astronomy, Arizona State University, Tempe, AZ 85287-1504;[2]
and Theoretical Division, Los Alamos National Laboratory, Los Alamos, NM 87545

AND

G. SHAVIV
Physics Department, Technion; and Asher Space Research Institute, IL 32000 Haifa, Israel
Received 1991 October 18; accepted 1992 January 3

ABSTRACT

Continuum and line-blanketed models for the photospheres of novae in the early stages of their outbursts are presented. The spherically symmetric, non–LTE, line blanketed expanding atmospheres are characterized by a very slow decrease of density with increasing radius. This feature leads to very large geometrical extensions so that there are large temperature differences between the inner and outer parts of the line-forming regions. The theoretical spectra show a large IR excess and a small Balmer jump which may be either in absorption or in emission. For the parameters considered ($T_{\rm eff} \approx 10^4$ K, $L = 2 \times 10^4\ L_\odot$, $\rho_{\rm out} \approx 3 \times 10^{-15}$ g cm^{-3}, $\dot{M} \approx 10^{-5}\ M_\odot$ yr^{-1} leading to a maximum expansion velocity of $v \approx 2000$ km s^{-1}, solar composition), most lines are in absorption. The effects of changes in the abundances of the heavy elements on the emergent spectra are discussed. We find that the strong unidentified features, observed in ultraviolet spectra of novae, are in actuality regions of transparency within the Fe "forest." We display ultraviolet spectra, obtained from the *IUE* archives, and do spectral synthesis of these spectra using our theoretical atmospheres.

Subject headings: novae, cataclysmic variables — stars: atmospheres — ultraviolet: stars

1. INTRODUCTION

Novae occur in cataclysmic variable binary systems in which a Roche lobe filling secondary is losing hydrogen-rich material through the inner Lagrangian point and, ultimately, onto the white dwarf primary. Theory requires and observations demand that the material falling onto the white dwarf mix, by some mechanism, with core material from the white dwarf. The accumulating shell of material on the white dwarf is unstable to a thermonuclear runaway (TNR) and hydrodynamic simulations of this phenomenon reproduce most of the observed features of the nova outburst: the typical amount of mass ejected, the kinetic energies of the ejecta, and the optical light curves. In addition, the simulations have led to the following predictions about the abundances: (1) that enhanced abundance levels of CNOMgNe nuclei should characterize the ejecta of fast novae; (2) that the isotopic ratios of the CNOMgNe nuclei should differ significantly from solar; and (3) that typical fast novae should have larger CNOMgNe enhancements than normal slow novae. Therefore, an accurate determination of the elemental abundances for nova ejecta is of paramount importance for understanding the cause and evolution of the outburst.

In recent years a large amount of high-quality spectral information, from X-ray to IR and radio wavelengths, has been obtained for novae in outburst (for reviews see Bode & Evans 1989 and the review articles by Cassatella & Gonzalez-Riestra 1990; Evans 1990; Gehrz 1990; Hjellming 1990; Ögelman 1990; Starrfield 1990, in Cassatella & Viotti 1990). However, the analyses of these data, in particular for the early stages of the outburst when the expanding envelope is still optically thick, are still very rudimentary. There are many spectroscopic features which appear during the evolution of a nova that are still unexplained and, in addition, there are strong lines in the ultraviolet that are not yet identified. Our problems are compounded because the techniques developed to analyze normal stars, whose atmospheres are in hydrostatic equilibrium, cannot be used on novae since nova atmospheres have very different density, temperature, and velocity structures from normal stars.

There are now more than 1200 spectra of novae in outburst in the *IUE* archives. These spectra cover both the early optically thick phase and the later nebular phase of the outburst. As a direct result of the analyses of the nebular spectra in the archives: (1) abundances have been determined for a large number of recent novae from their nebular emission lines; (2) two major compositional classes of outburst have been identified, one that occurs on an oxygen-neon-magnesium (hereafter, ONeMg) white dwarf and one that occurs on a carbon-oxygen (hereafter CO) white dwarf; (3) two classes of recurrent novae have been identified, one which has a giant for the mass-losing companion and one which has a compact, but also evolved, mass-losing companion; (4) evidence has been found for a high-temperature ($T > 2 \times 10^5$ K) source in the system at late times; (5) it has been determined that the outburst lasts longer in the UV than in the optical; and (6) it has been determined that the outbursts of the fastest classical and recurrent novae exceed the Eddington luminosity at maximum light (see Starr-

[1] Postal address: Department of Physics and Astronomy, Arizona State University, Tempe, AZ 85287-1504.
[2] Postal address.

field & Snijders 1987 and Starrfield 1992 for reviews of these data).

Of extreme importance is the fact that there are now observations of five LMC novae in the *IUE* archives. Some of the early data from their outbursts have been analyzed, but a model atmosphere study can, for example, provide improved distances to these novae and, therefore, to the LMC. Since there are analogous outbursts to four of the novae in the LMC (they include a moderate speed CO nova, a fast CO nova, a very fast CO nova, a fast ONeMg nova, and a recurrent nova), it is important to compare the outburst characteristics of the LMC novae to their galactic analogs in order to determine the effects of different metallicity in the accreted material on the evolution to outburst.

Up to now the determinations of abundances in novae ejecta have only been obtained from analyses of the optical, infrared, and ultraviolet emission-line fluxes obtained late in the outburst. These analyses use standard techniques developed for studying the spatially resolved emission lines in planetary nebulae. However, there also exist numerous *IUE* spectra of novae, obtained very early in the outburst, which have never been analyzed because the tools to do the analysis did not exist until recently. Nevertheless, there is a great deal of information about the nova outburst contained within these data. The expanding material is optically thick, however, and we must analyze these spectra with model stellar atmospheres calculated for expanding and not static material. One can then obtain the abundances of the ejected material from spectral syntheses of both the continuum energy distributions and line fluxes obtained from the early *IUE* spectra. These new abundances will be completely independent of abundances obtained from nebular emission-line analyses.

We emphasize the importance of utilizing a new method to obtain nova abundances since comparison of the results from two *different* abundance methods can provide an important check on both methods. No other astronomical object provides us with such an opportunity. Moreover, there are many novae, with spectra, in the *IUE* archives, that formed dust and, by combining the results from both techniques, it is possible to obtain abundance information before and after dust formation and possibly determine the composition of the dust. Finally, model atmosphere analyses of the *IUE* spectra allow us to determine the energy distributions of novae and obtain the effective temperature, the velocity and density distribution, and the radius of the expanding material as a function of time. These data will improve our knowledge of the energy budget of the nova outburst.

Therefore, in order to analyze the expanding, optically thick, atmospheres of novae, we have developed new methods that are appropriate for their structure. In this paper, we present our first results for non–LTE, blanketed, expanding, model atmospheres and calculate synthetic spectra for *IUE* observations of PW Vul 1984 No. 1. The atmospheric models are based on the idea that, during the early phases, the outer layers of novae in outburst behave like steady state, spherical, expanding winds (Bath & Shaviv 1976). Energy distributions based on this idea were calculated by Harkness (1983). However, his calculations were restricted to the continuum and the radial temperature distributions were kept fixed, i.e., he did not iterate to fulfill the energy equation. He was able to demonstrate the effects of the very low density in the outer layers which resulted in a dominance of scattering and, thereby, very large geometrical extensions. However, because of the limitations mentioned, the calculated energy distributions cannot be used for spectroscopic analyses. No other atmospheric modeling of this type for novae is known to us.

One of the input parameters to the code is the density distribution. In this paper we will use the hydrodynamic simulations of thermonuclear runaways in accreting white dwarf envelopes to obtain the density distribution and any deviations between the theoretical atmospheres and the observations will be useful in constraining the hydrodynamic simulations. Finally, the atmospheric calculations provide the opacity as a function of frequency and depth. These data can be used to obtain opacities that will be used, in turn, in the hydrodynamic simulations and possibly indicate the mechanism by which material is ejected during the late stages of the outburst.

In § 2 we present the ultraviolet data on both CO and ONeMg novae. In §§ 3 and 4, we list the assumptions made and outline the methods used for construction of our models. Since these atmospheres are very different, not only from normal stars but also from supernovae, the general properties of nova atmospheres are presented and discussed in § 5. In § 6 we present some synthetic spectra, and § 7 is devoted to the comparison with PW Vul. Section 8 provides a summary and discussion.

2. ULTRAVIOLET OBSERVATIONS OF NOVAE IN OUTBURST

There are now spectra of more than 20 novae in the *IUE* archives and five of the 20 have occurred in the LMC. Although the later stages of many of them have now been analyzed by nebular techniques (Starrfield 1992), there have been only cursory studies of the early spectra which were obtained at a time when most of the ejected material was still optically thick. In this section we exhibit and discuss some of the early spectra in preparation for our analyses to be presented in a later section.

2.1. *Carbon-Oxygen Novae: PW Vul and OS And*

In this subsection, we discuss two of the CO novae that have spectra in the *IUE* archives. They are PW Vul 1984 No. 1 and OS And 1986. We will return to PW Vul (1984 No. 1) later in this paper to show the results of our atmospheric analysis. Unfortunately, many of the early spectra of PW Vul 1984 No. 1 are overexposed in some wavelength regions which renders them very difficult to analyze. However, it is the slowest nova with spectra in the *IUE* archives and the thermonuclear runaway theory (see Starrfield 1989 and Shara 1989 for reviews) predicts that the abundances in the ejected material of such a nova should be very close to solar, as was found in the analysis of Saizar et al. (1991). Therefore, we decided to analyze the *IUE* spectra even when parts of the spectra on some days were overexposed.

Ultraviolet observations of PW Vul, with the *IUE* satellite, began on 1984 August 2, which was two days after discovery, and they continued until 1988 June 23. PW Vul reached its maximum visual brightness of $V = 6^{m}3$ on 1984 August 4 (JD 2,445,918; day 7 of the outburst). Papers discussing both *IUE* and optical spectra obtained during the nebular stage, which were used for an abundance analysis of the ejecta, have recently appeared (Saizar et al. 1991; Andreä, Drechsel, & Snijders 1991). The principal result of the Saizar et al. study is that all of the material in the ejecta has solar abundances except for nitrogen which is ~ 50 times solar. In contrast, Andreä et al. found that the CNO nuclei were considerably enhanced over solar. These two analyses obtained very different results for the

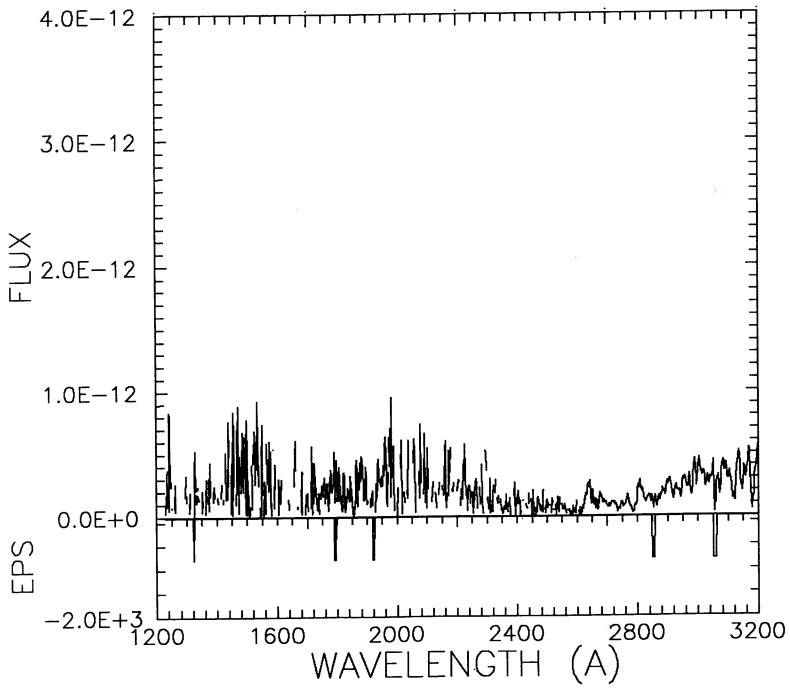

FIG. 1.—An *IUE* spectrum of Nova PW Vul 1984 No. 2 obtained on 1984 August 2. The image numbers are listed on the graph. The region below ~2500 Å is badly underexposed and probably none of the features in the SWP wavelength region (1200–1980 Å) are real. This spectrum has neither been dereddened nor has it been smoothed and the vertical lines in the SWP range indicate where the fluxes for some pixels would lie below zero. The lower plot gives the "error" or ϵ vector as a function of wavelength. The wavelength regions where ϵ is negative have been so marked by the reduction software because they were overexposed or there were cosmic-ray "hits." The LWP wavelength region shows Mg II λ2800 with a P Cygni profile and, probably, Fe II λ2633 is also present.

abundances in the ejecta because they derived different values for the electron temperature and density in the expanding shell at the times when the spectra were taken. These two analyses taken together emphasize the difficulties in nebular methods and demand an abundance determination using another and independent method. Nevertheless, the gross differences between the spectral evolution of CO and ONeMg novae are so great that there is no doubt, whatsoever, that these two distinct compositional classes of novae exist.

It is the purpose of this paper to present this new method and to apply it to the early spectra of PW Vul.

The first *IUE* spectrum of PW Vul (SWP 23576 plus LWP 3911: 1984 August 2) is shown in Figure 1. It was obtained before maximum light in the ultraviolet and shows a rather flat continuum in the short wavelength range which slowly rises to the red at longer wavelengths. None of the spectra, shown in this section of the paper, have been corrected for reddening. It is clear that the SWP spectrum was badly underexposed and these data, plus those to be presented below, indicate the difficulty of obtaining well-exposed *IUE* spectra of strongly time variable objects. We have not smoothed these spectra and the vertical, isolated lines occur when the value of the flux is negative at a particular wavelength. While it is not possible to identify any features at short wavelengths, Mg II λ2800 is definitely present in the LWP spectrum and shows a P Cygni profile indicating material has been ejected. It also appears that Fe I λ2633 is present.

Figure 2 shows the spectrum obtained on 1984 August 5 (SWP 23604 plus LWP 3941). This spectrum, which shows a continuum steeply rising to the red, is very characteristic of the early spectra of novae which have ejected enough material so that they are optically thick at radii of $\sim 10^{12}$ cm. Later in this section, we will discuss the early spectra of fast ONeMg novae in which the amount of ejected material is (apparently) smaller and the envelope is optically thin in the lines before the expanding material has reached 10^{12} cm. In the analysis in § 5, we also will show that while the steeply rising red continuum mimics that of a late-type star, in fact, the effective temperature of the atmosphere used to reproduce this continuum exceeds 10^4 K. The reason for this result is that the radial extent of a nova atmosphere is very large; much larger than is found for SN II.

Below each spectrum we have also plotted the error vector (ϵ) which is provided by the *IUE* reduction software. It has a value of +100 at all wavelengths where there is no obvious problem with the data. However, it is negative where problematic points have been flagged by the reduction software and can reach a value of −2000 for very strongly overexposed wavelengths. It is clear, from examining the error vector shown in Figure 2, that wavelengths from ~2800 to 3150 Å are overexposed. This is a common problem in early novae spectra since they exhibit large variations in their fluxes as one goes from short to long wavelengths. Normally, one must obtain multiple spectra with exposure times chosen for specific spectral regions. Unfortunately, multiple spectra, with a variety of exposure times, were not obtained for PW Vul near maximum light and we are forced to display, and attempt to analyze, spectra that are overexposed. We do not analyze all regions of these spectra with our model atmospheres since a "good" fit to the fluxes at these wavelengths is meaningless, but the time evolution still provides an estimate of the direction of evolution of the effective temperature of the expanding shell.

As will be shown, most of the emission features which appear in Figure 2 are not really emission features but regions of transparency between overlapping metal lines. However, Mg II λ2800 is present and shows a P Cygni profile and

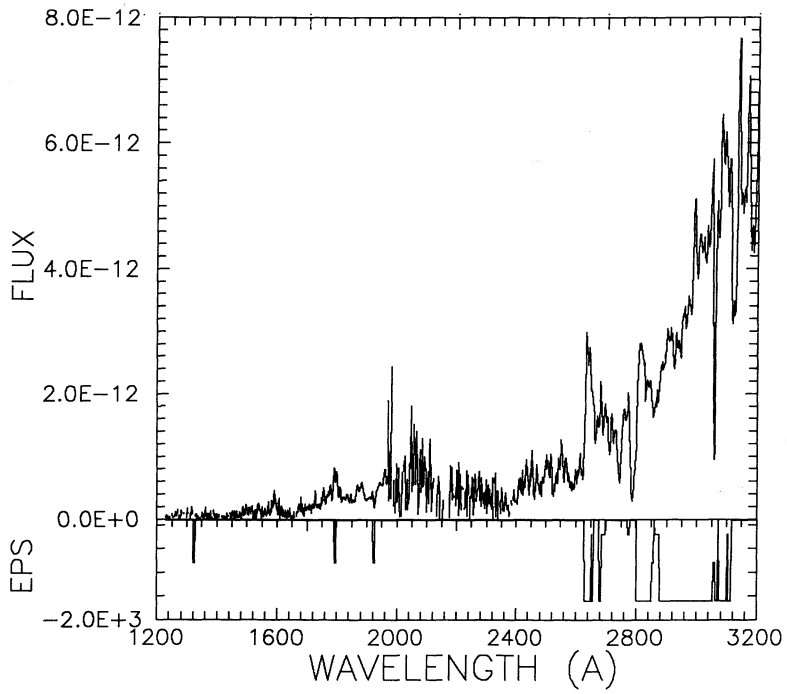

FIG. 2.—Same as Fig. 1 but obtained on 1984 August 5, 3 days after the spectrum shown in Fig. 1. Note the very large increase in the long-wavelength flux. Unfortunately, as can be seen from the ϵ vector, most of the spectrum longward of 2800 Å is overexposed and, therefore, virtually useless for our analysis. It is very difficult to obtain spectra of novae with all wavelengths optimally exposed. In general, it is necessary to obtain multiple exposures with differing exposure times and then combine these spectra. However, only one spectrum was obtained on this date.

Fe I $\lambda\lambda$2633, 2668 are also present. Unfortunately, the peaks of these lines are overexposed. Note that the total flux emitted in the UV has increased very strongly in the 3 days since the first spectrum.

Figure 3 shows the spectrum as it appeared on 1984 August 18 (SWP 23717 plus LWP 4017). Unfortunately, now most of the wavelength region between 1700 and 2000 Å is overexposed rendering this part of the spectrum useless as is also the case for wavelengths longer than 2700 Å. In addition, the Fe I and Mg II lines in the LWP camera are overexposed. Nevertheless, the fluxes at well-exposed wavelengths show that the nova has decreased in brightness since the time that the spectra shown in Figure 2 were obtained. Therefore, UV maximum occurred some time between that of Figure 2 and Figure 3 and after optical maximum (Austin et al. 1990).

The second nova that we discuss is OS And 1986. It was a moderate-speed CO nova whose UV spectral features, at early times, closely resembled those in the spectra of PW Vul. It was originally discovered by Suzuki (1986) at $m_{pv} = 8.0$ on 1986 December 5, and it reached maximum visual brightness of $V \approx 6^{m}.3$ on 1986 December 9 (U.T.). Ultraviolet observations with the *IUE* satellite began on 1986 December 9 and continued until the discovery of SN 1987A in late February of 1987. After that time, spectra were obtained on an infrequent basis. Fortunately, most of the early spectra were not overexposed, so that we can obtain an accurate picture of the early evolution of this nova. Analysis of the late time *IUE* and optical spectra is now underway (Austin et al. 1992) and our results indicate that all of the CNO nuclei are enhanced in this nova. Austin et al. use the observed ratio of He II λ4686 to He II λ1640 to determine a reddening of $E(B-V) = 0.07$. However, the spectra that we display in this section have not been corrected for reddening.

The first spectrum of OS And (Fig. 4) was obtained on day 343 of 1986 (SWP 29837 plus LWP 9667) and was the day that peak brightness was reached in the optical. Again, just as for PW Vul, it shows a very cool continuum comprised mainly of overlapping absorption from metal lines. The P Cygni feature at 1860 Å is probably Al III although that seems too high an ionization state to be seen so early in the outburst in a CO nova with an optically thick expanding shell. The line at 2610 Å is Fe II as is the strong feature at $\sim$3000 Å. Note the very strong P Cygni profile for Mg II λ2800. The spectrum is very poorly exposed between $\sim$2000 and 2300 Å, and we do not claim that any of the features in that wavelength interval are real.

Although we obtained other spectra, the next spectrum that we display in this paper was taken on 1986 day 351 (Fig. 5: SWP 29894 plus LWP 9718). It shows that there has been a great deal of evolution of the nova over the 8 day interval shown in Figures 4 to 5. The nova has continued to brighten in the ultraviolet, although peak brightness in the optical was reached at the time Figure 4 was obtained. Again, this is a common feature of all well-studied novae: peak brightness in the ultraviolet occurs after peak brightness in the optical (Austin et al. 1991). Mg II λ2800 is now the strongest line in the spectrum and has grown in intensity by nearly a factor of 10 in the 8 day interval. In addition, the P Cygni absorption feature has become much less prominent. While the Fe II lines are still present, they have become much less important and the slope of the continuum has started to flatten. The prominent feature at $\sim$2000 Å falls in the poorly exposed region of the LWP camera, and we do not feel that it is real. In the SWP spectrum we are now able to indentify C II λ1335, N IV] λ1486, C IV λ1550, He II λ1640, N III] λ1750, Al III λ1857, and C III λ1909. It is clear that the region where the photosphere is formed has

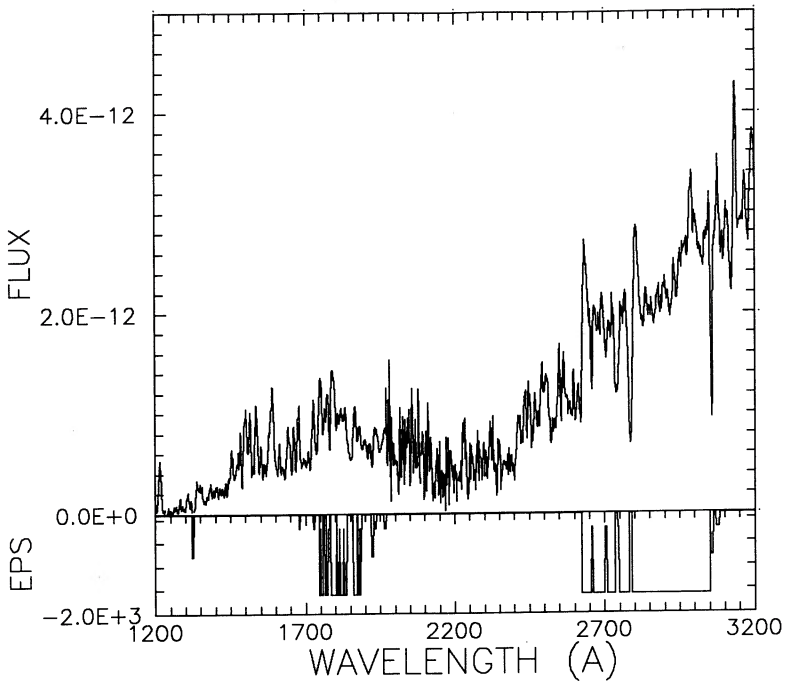

FIG. 3.—Same as Fig. 1 but obtained on 1984 August 18. It is clear that the nova has dropped in brightness over the 2 week interval from Fig. 2 to this figure. Again, there are major regions of the spectrum that are overexposed. However, it is also clear that the expanding material is becoming hotter since the short-wavelength region is becoming brighter with respect to the long-wavelength region. While the region around 2200 Å is somewhat underexposed, it is obvious that this nova is reddened.

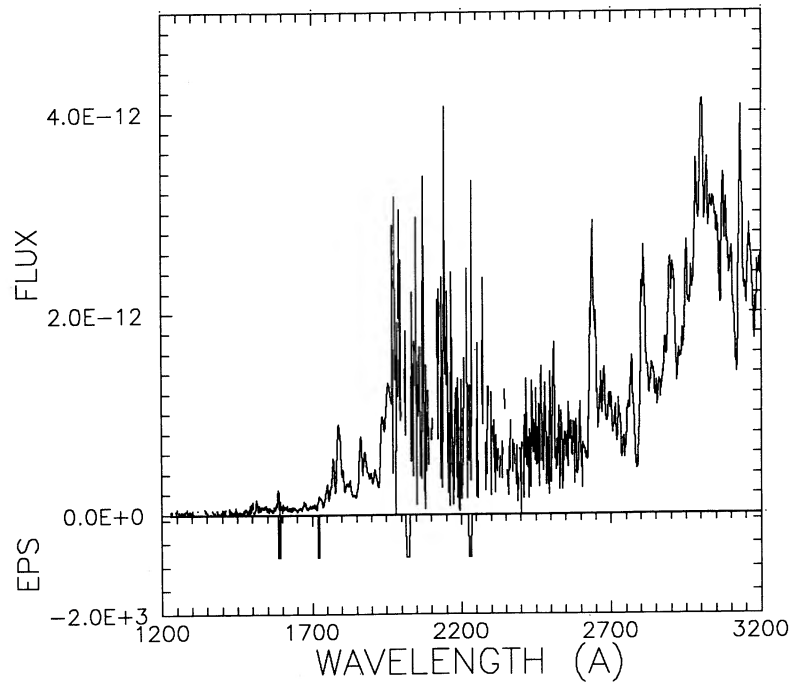

FIG. 4.—This is an *IUE* spectrum of Nova OS And 1986 obtained on 1986 December 9, just after discovery. If we compare this spectrum to those of PW Vul, then we see that the expanding material is (probably) somewhat hotter than the material shown in Fig. 3, since the continuum is somewhat flatter. All of the features in the long-wavelength camera show P Cygni profiles which indicate that mass loss is occurring. The most prominent lines are Mg II λ2800 and Fe II λ2610 and $\sim$3000 Å.

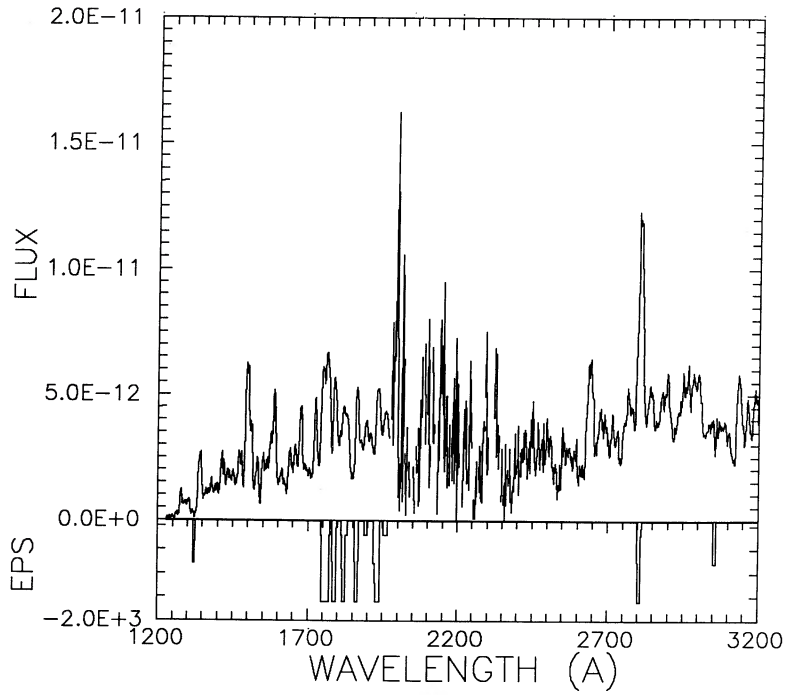

FIG. 5.—Same as Fig. 4 but obtained on 1986 December 17. Note how the continuum has become flatter and the ionization has increased indicating that the material is increasing in temperature. Mg II λ2800 has also increased in intensity by nearly a factor of 10 in the 8 day interval. While the Fe II lines are still present, they have become much less important. The prominent feature at ~2000 falls in the poorly exposed region of the LWP camera, and we do not feel that it is real. In the SWP spectrum we are now able to identify C II λ1335, N IV] λ1486, C IV λ1550, He II λ1640, N III] λ1750, Al III λ1857, and C III λ1909.

moved inward to deeper and hotter layers and a significant fraction of the expanding layers have become optically thin.

Ten days later there has been a much larger change in the observed spectrum. Figure 6 (SWP 29980 plus LWP 9794) was obtained on 1986 day 361 and shows that the continuum is now rising to the blue so that it must be produced by material that is hotter than that seen in the previous two spectra. Mg II λ2800 has dropped in strength and the strongest line in the spectrum is now N III] λ1750. N V λ1240 is present which indicates that there is an underlying high-temperature source in

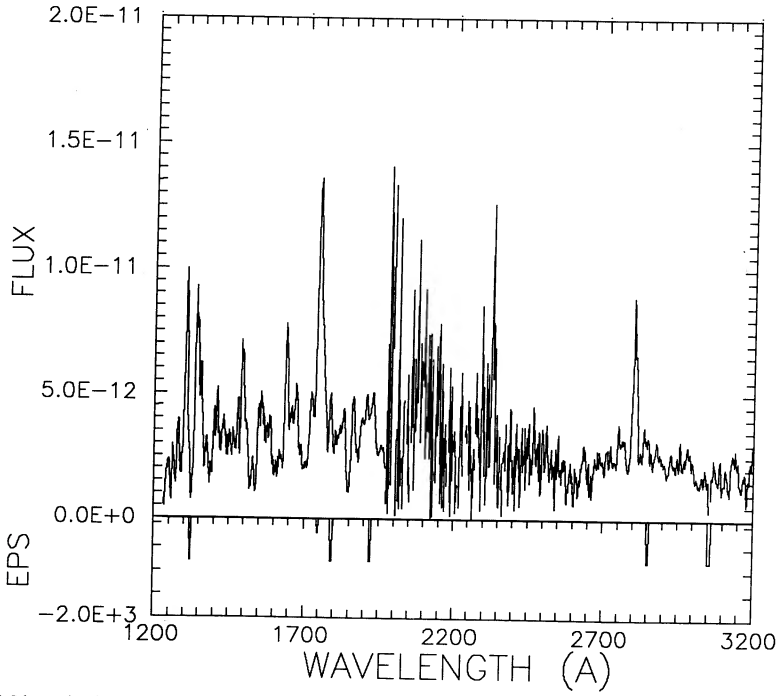

FIG. 6.—Same as for Figs. 4 and 5 but obtained 10 days later, on December 27. The material producing the spectrum has now become significantly hotter, and the strongest line is N III] λ1750. N V λ1240 is present and strong which indicates that there is an underlying high temperature source in this system.

the system. However, we still see a wide variety of ions and ionization states as is commonly observed in optical spectra of novae.

2.2. *Oxygen-Neon-Magnesium Novae*

A number of fast ONeMg novae have also been observed in outburst with the *IUE* satellite. These include V693 CrA, V1370 Aql, LMC 1990 No. 1, Her 1991, and Sgr 1991. Papers describing and analyzing the nebular spectra in the *IUE* archives for some of these novae have appeared (Williams et al. 1985; Snijders et al. 1987; Sonneborn, Shore, & Starrfield 1990; Shore et al. 1992) and, since they show representative early spectra of these novae, we do not reproduce any spectra in this subsection. In addition, a slow ONeMg nova, QU Vul 1984 No. 2, has also been studied with the *IUE* satellite (Saizar et al. 1992). We will not analyze the early spectra of these novae in this paper but discuss their spectra both for completeness and, in addition, to contrast their spectral features and evolution with that of the CO novae.

The earliest spectra of V693 CrA (Williams et al. 1985), LMC 1990 No. 1 (Sonneborn, Shore, & Starrfield 1990), and Srg 1991 appear very different from the spectra presented in the previous section. This is the case even when the spectra are obtained at the time of maximum light in the optical and prior to the time of maximum light in the ultraviolet (Sonneborn, Shore, & Starrfield 1990; Austin et al. 1990). The differences are striking and are caused by the presence of high-ionization lines such as N v λ1240, Si iv λ1400, C iv λ1550, and Al iii λ1860 characteristic of an optically thin gas. In addition, the continuum slopes very strongly to the blue even before the nova is dereddened. We suggest that the differences in appearance between the CO and ONeMg novae must be caused by differences in the amount of material ejected during the outburst. We note that a classical CO nova ejects sufficient material for the expanding envelope to remain optically thick until it reaches a radius of $\approx 10^{12}$ cm. In contrast, a significant fraction of the material ejected by a fast ONeMg nova has become optically thin by the time that the layers have reached $\approx 10^{12}$ cm implying that not as much material was ejected in an ONeMg outburst. Another class of novae that show a similar spectral evolution to the ONeMg novae are recurrent novae (RNs). For example, the first ultraviolet spectra obtained for U Sco and LMC 1990 No. 2 (both RNs) were very similar to those of fast ONeMg novae (Williams et al. 1981; Shore et al. 1991) and not to those of the CO novae displayed in the previous subsection. Analyses of recurrent novae show that less material is ejected in the outburst than found for CO novae (Williams et al. 1981; Shore et al. 1991).

Nevertheless, there is one slow ONeMg nova in the *IUE* archives: QU Vul 1984 No. 2 (Saizar et al. 1992). It was discovered at $V \approx 6^{m}.8$, on 1984 December 22.13 UT. It reached a maximum apparent magnitude of $5^{m}.6$, on 1984 December 25.0 UT. Although the infrared observations of Gehrz and his collaborators found very large ejection velocities, its rate of decline in the optical has been very slow (Gehrz 1988). In addition, as can be seen in spectra displayed by Stryker et al. (1988), it did display an optically thick shell at maximum light with a radius of $\approx 10^{12}$ cm. An analysis of the nebular spectra is in progress (Saizar et al. 1992), and we will use our model atmospheres to analyze the early spectra in a future paper. Therefore, ONeMg novae can eject as much material as CO novae.

3. MODEL ASSUMPTIONS

Following the discussion of Bath & Shaviv (1976), we consider nova photospheres to be spherical and expanding but stationary configurations. Therefore, we assume that all time-dependent terms both in the hydrodynamics and in the radiative transfer equation can be neglected and all quantities depend only upon the radial coordinate (except for the specific intensity of the radiation field which, in addition, depends on the angle to the radial direction). These assumptions seem to be justified since the hydrodynamic time scale is much longer than the time scales for photon escape and for the establishment of excitation and ionization equilibria. In addition, since the abundant radioactive species have very long half-lives so that a negligible amount of energy is deposited into the atmosphere by radioactive decays, we assume radiative equilibrium in the Lagrangian frame. Using the results from hydrodynamic calculations of the consequences of thermonuclear runaways in accreted envelopes on white dwarf stars (see Shara 1989 & Starrfield 1989, 1992 for reviews), we assume that the density varies according to a power law, $\rho \propto r^{-n}$, and the expansion velocity is given by $v = \dot{M}/4\pi r^2 \rho$, with $\dot{M}$ being the mass-loss rate.

We assume that $\dot{M}$ = constant with respect to both the radial distance and the time (Bath & Shaviv 1976). This is a crucial assumption because it determines the run of velocity in the atmosphere. Detailed numerical hydrodynamic calculations, which assume a diffusion approximation for the radiative transfer, show that the assumption of constant $\dot{M}$ is reasonable.

We expect departures from local thermodynamic equilibrium (LTE) to be important in nova photospheres because of the low densities in the expanding shell. Therefore we include, self-consistently, the non–LTE effects of important species (H i, Mg ii, and Ca ii) in the model construction, i.e. in the radiative transfer equation, the radiative equilibrium equation and in determining the ionization equilibria of all the species. The early spectra of novae show a large number of lines in the UV wavelength range (1200–3400 Å: see § 2) and the effective temperature is high so that a significant fraction of the total flux emerges in the UV. It is clear that proper models of nova photospheres must include line blanketing by a large number of UV lines to reproduce the observed spectra. Furthermore, for abundance determinations we have to use single lines and need to know the dependence of the line profiles on the parameters of the envelope. For this reason we include in the model construction and the computation of the synthetic spectra $\sim 10^5$ metal UV lines in addition to the non–LTE lines. Details of how the lines are selected are given later.

We characterize the models by the following parameters: (1) the reference radius R, which refers to the radius where either the optical depth in absorption or extinction at 5000 Å is unity, (2) the effective temperature $T_{\rm eff}$, which is defined by means of the luminosity, L, and the reference radius ($T_{\rm eff} = (L/4\pi R^2\sigma)^{1/4}$, where σ is Stefan's constant, (3) the density parameter, n, (4) the mass-loss rate, $\dot{M}$, (5) the density, $\rho_{\rm out}$, at the outer edge of the envelope, (6) the line scattering parameter (see below), and (7) the element abundances.

Typical values of n for nova envelopes are $n \approx 3$, as determined from the hydrodynamic simulations of the nova outburst (Starrfield 1992). Consequently, the decrease in density with increasing radius is relatively slow and the outer boundary condition, $\rho_{\rm out}$, has a nonnegligible effect on the entire structure of the expanding envelope. This is in contrast to the

situation in compact atmospheres or even supernovae and red giant photospheres.

4. MODEL CONSTRUCTION

For the calculation of the models and the synthetic spectra, we follow the same philosophy as we have used for supernova photospheres since many of the problems in simulating nova envelopes are similar to the problems encountered in simulating SN envelopes. In fact, our nova model construction is identical to the method developed for SN (Hauschildt, Shaviv, & Wehrse 1989; Hauschildt, Best, & Wehrse 1991; Hauschildt 1991). We solve the combined radiative transfer, radiative equilibrium, and non–LTE rate equations for an expanding shell with given density and velocity laws (which replace the hydrodynamic equations). An accurate description of line blanketing and the Lagrangian radiation field requires the solution of the radiative transfer equation at a large number of wavelength points. Up to 1700 wavelength points were used in the models reported in this paper. The use of the complete linearization method (Auer & Mihalas 1969) is not feasible under these conditions because the CPU time for this method scales with the cube of the number of wavelength points. Therefore, we used a combination of a Newton-Raphson iteration for the temperature structure and a fixed point iterative scheme for the departures from LTE (see below). This scheme scales only linearly with the number of wavelength points and the number of iterations required for convergence is relatively small.

4.1. *Construction of the Radial Grid*

The density distribution is found in the beginning of each iteration by integrating the equations:

$$\frac{dr}{d\tau_{\rm std}} = -\frac{1}{(\kappa_{\rm std} + \sigma_{\rm std})} \tag{1}$$

on a prescribed optical depth grid $\tau_{\rm std}$, where $\tau_{\rm std}$ is the optical depth in the continuum at a wavelength of 5000Å. The temperature structure $T(\tau_{\rm std})$ and the run of the non–LTE departure coefficients (see below) are obtained from the previous model iteration. The value of the outer radius is iterated to satisfy the condition

$$r(\tau_{\rm std} = 1) = R\ . \tag{2}$$

In equation (1), r denotes the radial coordinate, $\kappa_{\rm std}$ the absorption coefficient at 5000 Å and $\sigma_{\rm std}$ the scattering coefficient at 5000 Å.

4.2. *Radiative Transfer*

The spherically symmetric radiative transfer equation in the Lagrangian ("comoving") frame is given by (see Mihalas & Weibel-Mihalas 1984)

$$\gamma(\mu+\beta)\frac{\partial I}{\partial r} + \frac{\partial}{\partial \mu}\left\{\gamma(1-\mu^2)\left[\frac{(1+\beta\mu)}{r} - \gamma^2(\mu+\beta)\frac{\partial \beta}{\partial r}\right]I\right\} - \frac{\partial}{\partial v}\left\{\gamma\left[\frac{\beta(1-\mu^2)}{r} + \gamma^2\mu(\mu+\beta)\frac{\partial\beta}{\partial r}\right]vI\right\} + \gamma\left\{\frac{2\mu+\beta(3-\mu^2)}{r} + \gamma^2(1+\mu^2+2\beta\mu)\frac{\partial\beta}{\partial r}\right\}I = \eta - \chi I\ . \tag{3}$$

In equation (3), μ is the cosine of the angle between a ray and the direction normal to the surface, v the frequency, $I = I(r, \mu, v)$ denotes the specific intensity at radius r and frequency v in direction arccos μ in the Lagrangian frame. The matter velocity $v(r)$ is measured in units of the speed of light c, $\beta(r) = v(r)/c$, and γ is given by $\gamma = 1/(1-\beta^2)^{1/2}$. The sources of radiation present in the matter are described by $\eta = \eta(r, v)$ and $\chi = \chi(r, v)$ denotes the extinction coefficient; η contains contributions from scattering terms proportional to the mean intensity J of the form $\sigma\bar{J}$ (where $\bar{J}$ is the mean intensity averaged over the line profile) which are explicitly treated in the radiative transfer. The radiation fields derived from the solution of equation (3) incorporate all relativistic effects, in particular advection and aberration. However, these effects are small in the models presented in this paper in contrast to the situation found in SN envelopes (Hauschildt et al. 1991).

The numerical procedure used for the solution of equation (3) is based on the discrete-ordinate-matrix-exponential (DOME) method (Schmidt & Wehrse 1987) for fast, expanding configurations (Hauschildt & Wehrse 1991). Appendix A gives a short summary of the DOME method. The accuracy of the solution of equation (3), obtained with the DOME code, was checked by comparison with the results calculated with a short characteristic-accelerated Λ-iteration method (Olson & Kunasz 1987) for the solution of equation (3) (Hauschildt 1992). We found that the differences between the two solutions were always smaller than a few percent for all wavelengths and optical depths and that the relative differences between the emergent spectra, i.e., the shape of the spectrum, were always smaller than $\sim 10^{-3}$.

4.3. *Temperature Correction Procedure*

The kinetic temperature (in the following simply called temperature) distribution is iterated so as to fulfill the radiative equilibrium equation in the Lagrangian frame,

$$\int_0^\infty \kappa_\lambda(B_\lambda - J_\lambda)d\lambda = 0\ , \tag{4}$$

where

$$J = r^2/2\int_0^\infty\int_{-1}^1 I_\lambda\, d\mu\, d\lambda$$

and B_λ denotes the Planck function scaled by r^2, or the equivalent condition for the wavelength integrated Eddington flux:

$$\frac{\partial H}{\partial r} + \beta\frac{\partial J}{\partial r} + \frac{\beta}{r}(J-K) + \gamma^2\frac{\partial\beta}{\partial r}(J+K+2\beta H) = 0\ , \tag{5}$$

where

$$H = r^2/2\int_0^\infty\int_{-1}^1 \mu I_\lambda\, d\mu\, d\lambda\ ,$$

$$K = r^2/2\int_0^\infty\int_{-1}^1 \mu^2 I_\lambda\, d\mu\, d\lambda\ .$$

An iterative procedure to compute the temperature structure, fulfilling equations (4) and (5), can be obtained in the following way (Hauschildt et al. 1991). The value of the Eddington flux H, as measured by an external observer, $H_{\rm obs}$, is a given model parameter. Using the transformation formulae between the Lagrangian and the Eulerian systems for the wavelength integrated moments of the radiation field (e.g.,

Mihalas & Weibel-Mihalas 1984),

$$J_{\rm obs} = \gamma^2(J + 2\beta H + \beta^2 K)\,, \tag{6}$$

$$H_{\rm obs} = \gamma^2[(1 - \beta^2)H + \beta(J + K)]\,, \tag{7}$$

$$K_{\rm obs} = \gamma^2(K + 2\beta H + \beta^2 J) \tag{8}$$

(replace β by $-\beta$ for the inverse transformation), we can compute the Euler system radiation field moments (denoted by the subscript "obs") from the corresponding quantities in the Lagrangian frame which are assumed to be known from a previous solution of the radiative transfer equation (3) for a (large) number of wavelength points. If we assume that the geometry factors, $f_{\rm obs} \equiv J_{\rm obs}/H_{\rm obs}$, and $g_{\rm obs} \equiv K_{\rm obs}/H_{\rm obs}$, are not sensitive to the temperature, we can compute an improved estimate for the Eddington flux in the Lagrange frame $H^{(1)}$ at $\tau_{\rm std} = 0$ by means of the expression

$$H^{(1)} = \gamma^2\{(1 + \beta^2)H_0 - \beta H_0(f_{\rm obs} + g_{\rm obs})\}\,, \tag{9}$$

where $H_0 = L/(4\pi)$.

Using $H^{(1)}$ as an initial condition and assuming that the Lagrangian frame geometry factors $f \equiv J/H$ and $g \equiv K/H$ are only weakly dependent on the temperature, we can solve equation (5) as an ordinary differential equation by means of standard numerical methods. This procedure gives the improved run of $H^{(1)}(\tau_{\rm std})$ in the Lagrangian frame. Experience has shown that the radiative equilibrium condition, equation (4), is numerically well-conditioned in the optically thin parts of the atmosphere $\tau_{\rm std} < \tau_s$ (with $\tau_s \approx 1$) but, in the optically thick parts of the photosphere $\tau_{\rm std} \geq \tau_s$, the equivalent condition for the total flux,

$$H(\tau_{\rm std}) - H^{(1)}(\tau_{\rm std}) = 0 \tag{10}$$

is better behaved (numerically). We define, therefore, a radiative equilibrium function F by

$$F = \begin{cases} \displaystyle\int_0^\infty \kappa_\lambda[B_\lambda(r) - J_\lambda(r)]d\lambda & \text{for} \quad \tau < \tau_s \\ \displaystyle H^{(1)}(r) - \int_0^\infty H_\lambda(r)d\lambda & \text{for} \quad \tau \geq \tau_s\,. \end{cases} \tag{11}$$

F is a vector of length N_s, where N_s is the number of discrete shells included in the model. We define the Jacobian matrix of F with respect to the corresponding vector T of the electron temperature as

$$[\boldsymbol{DF}(T)]_{ij} = \begin{cases} \displaystyle\int_0^\infty \kappa_\lambda\left[\frac{\partial B}{\partial T}(T_j)\delta_{ij} - \frac{\partial J_i}{\partial T_j}\right]d\lambda & \text{for} \quad \tau < \tau_s \\ \displaystyle\frac{\partial H_{0,i}}{\partial T_j} - \int_0^\infty \frac{\partial H_i}{\partial T_j}\,d\lambda & \text{for} \quad \tau \geq \tau_s\,, \end{cases} \tag{12}$$

where we have neglected the $\partial\kappa/\partial T$ derivative for simplicity. In equation (12) i and j refer to the shells r_i and r_j, respectively. The Newton-Raphson formula for the improved temperature structure is then given by

$$T^{(1)} = T_0 - [\boldsymbol{DF}(T_0)]^{-1}F(T_0)\,, \tag{13}$$

where T_0 denotes the actual temperature vector and $T^{(1)}$ the corrected vector. The computation of the Jacobian is performed using the results of the DOME radiative transfer method and uses only a small amount of computer time (see the following section).

4.4. *Computation of the Jacobian Matrix*

One advantage of the DOME method is that the Jacobi matrix, needed for the temperature correction procedure, can be calculated very easily. We first write equation (3) in the form (see Hauschildt & Wehrse 1991 for details)

$$e\frac{\partial I}{\partial r} + \frac{\partial}{\partial \mu}(fI) + g\frac{\partial}{\partial \lambda}(\lambda I) + hI = \eta - \chi I\,, \tag{14}$$

where the auxiliary functions are given by

$$e(r, \mu) = \gamma(\mu + \beta) \tag{15}$$

$$f(r, \mu) = \gamma(1 - \mu^2)\left[\frac{1 + \beta\mu}{r} - \gamma^2(\mu + \beta)\frac{\partial \beta}{\partial r}\right], \tag{16}$$

$$g(r, \mu) = \gamma\left[\frac{\beta(1 - \mu^2)}{r} + \gamma^2\mu(\mu + \beta)\frac{\partial \beta}{\partial r}\right], \tag{17}$$

$$h(r, \mu) = \gamma\left[\frac{\beta(1 - \mu^2)}{r} + \gamma^2(1 + \mu^2 + 2\beta\mu)\frac{\partial \beta}{\partial r}\right]. \tag{18}$$

The solution of equation (14) with the DOME method can be written in the form $\boldsymbol{U}I = Q$, where the matrix $\boldsymbol{U}$ contains terms from the discretized differential operator and the scattering part of the source function, I denotes the discretized intensity vector, and Q the thermal part of the source function. Differentiation of equation (14) with respect to the temperature T_i in shell i gives

$$e\frac{\partial I'}{\partial r} + \frac{\partial}{\partial \mu}(fI') + g\frac{\partial}{\partial \lambda}(\lambda I') + hI' = \eta' - \chi I' - \chi' I\,, \tag{19}$$

where the prime denotes differentiation with respect to T. Equation (19) has the same form as equation (14) but with a different right-hand side, so we can write the solution of equation (19) in the form

$$\boldsymbol{U}\frac{\partial I}{\partial T_i} = \tilde{Q}\,. \tag{20}$$

The matrix $\boldsymbol{U}$ has a block-tridiagonal structure and the linear system $\boldsymbol{U}I = Q$ can be solved efficiently by LU decomposition and subsequent backsubstitution. Thereafter, we can reuse the LU decomposed matrix $\boldsymbol{U}$ to compute $\partial I/\partial T_i$ very efficiently by backsubstitution. This same matrix can then be used to compute the matrices needed in the temperature correction procedure. A similar approach could be used to compute other Jacobians of the radiative transfer equation, e.g., those that treat the electron pressure, P_e.

4.5. *Treatment of the Non-LTE Levels*

The level populations for H (10 levels), Ca II (five levels), and Mg II (three levels) are obtained from the non-LTE rate equations, whereas for the remaining levels (and other species) the Boltzmann population distribution at the local kinetic temperature is assumed. The atomic data for H I were taken from Johnson (1972), the data for Mg II, and Ca II were taken from Shine (1973) and Shine & Linsky (1974), respectively. The ionization equilibrium is solved for the non-LTE species and the ionization stages I–III of He, C, N, O, Si, S, Fe, Al, Na, K, Ti, Sc, Mn, and Cr. In order to derive consistent values of the radiation field and the departure coefficients $b_i \equiv n_i/n_i^*$, where n_i and n_i^* denote the non-LTE and LTE occupation numbers of the levels treated in non-LTE, we use the equivalent two-

level atom (ETLA) method (e.g., Mihalas 1978) to compute the non–LTE line source function and iterate for the b_i. All permitted transitions of the non–LTE species (55 lines for H I, two lines for Mg II, and five lines for Ca II) are treated in this way. We have checked the model atom for H I by using 15 non–LTE levels and found only small differences in the departure coefficients for the first six to eight levels as compared to the results of the 10 level H I model atom.

4.6. *LTE Continuum and Line Opacities*

The contributions to the continuous opacity from bound-free and free-free transitions of all important absorbers, as well as Rayleigh and Thomson scattering, are taken into account with the cross sections as compiled by Mathisen (1984). For the calculation of the line opacity we use the line list of Kurucz & Peytremann (1975) in which a new list of Fe II lines (Kurucz 1988) was incorporated. The entire list contains close to 2 million lines; however, not all of them are important for the case at hand. Therefore, before every temperature iteration, a smaller list (which may contain up to $\sim$150,000 entries) is formed from the original list. First, a continuum level is chosen, usually at $\tau_{\rm std} \approx 0.01$. Then, using the density and temperature for this level the absorption coefficient in the line center, κ_l, is calculated for every line and compared to the corresponding continuum absorption coefficient, κ_c. A line is transferred to the "small list" if the ratio κ_l/κ_c is larger than a prespecified value p (usually 10^{-4}). In the subsequent radiative transfer calculations, all lines selected in this way are taken into account as individual lines, all others from the large line list are neglected. This selection procedure is repeated at *every* iteration in order to always include the most important lines, even when the temperature stratification changes significantly.

The number of lines which are included by the line-selection procedure is a function of both p and the continuum level at which the above criterion is applied. The values of p and $\tau_{\rm std}$ were chosen so that (*a*) a minimum number of lines would be selected and (*b*) reducing p (which would include more lines) would not change either the emergent spectra or the temperature stratification in any noticeable way. Tests of the selection procedure included up to 5×10^5 lines and three depth points. These tests showed that values of $p = 10^{-4}$, $\tau_{\rm std} \approx 10^{-2}$, and $\sim 10^5$ lines were both sufficient and *necessary* for reliable modeling of the spectra. For example, the flux differences, ΔH, between the model including 5×10^5 lines and the model including only 10^5 lines are very small, $\Delta H/H < 10^{-5}$ for all depths and frequencies. With the above selection procedure, we can simultaneously select the most important lines and restrict the total number of lines included so that the problem remains computationally feasible without necessitating further major approximations. The effects of interlocking lines and multiple scattering are automatically taken into account. Nevertheless, we must also note that it is not clear to what extent the tables prepared by Kurucz & Peytremann (1975) are complete for nova conditions so that a large number of transitions, in particular for higher ionization stages, may be missing. However, we emphasize that the important strong lines are well-known and the missing lines would probably be very weak. As we have demonstrated above, including these lines would not change our results significantly.

The line profiles are assumed to be Gaussian. The exact shape is not important since the Doppler shifts caused by differential expansion within the ejected layers are always much larger than the line widths due to thermal and collisional broadening (see also Eastman & Kirshner 1989). Next, we assume that all levels (except the levels treated in non–LTE) are populated according to the Boltzmann distribution of the local temperature (see above). In the solution of the radiative transfer equation, a fraction, α, of the line absorption coefficient is assumed to contribute to the absorption coefficient ("true absorption") while the remaining fraction, $(1 - \alpha)$, is included as part of the line scattering. In reality, α varies both from line to line, and with depth, so that its actual determination demands a full non–LTE calculation. We circumvent this problem by treating α as a free parameter. We found in our test calculations that changing α over a range from 0.01 to 0.9 did not change the flux at most UV wavelengths by more than a few percent. Therefore, we adopt here an "average value" of α for all lines and depths of 0.5.

4.7. *Model Iteration*

The model iterations are performed in the following way: first we construct the radial grid corresponding to the prescribed optical depth grid as described in the previous sections. This is redone at the beginning of each model iteration because, in the early stages of the model construction, the variation with depth of both the temperature and the departure coefficients may change significantly from iteration to iteration. Afterward, the line selection algorithm outlined above is carried out and the selected lines are stored. The radiative transfer equation (3) is then solved for all wavelengths and optical depths and the temperature correction matrix is constructed. The new radiation field is then used to compute new estimates of the radiative rates for all transitions (line and continuum) treated in non–LTE. The new values for the radiative rates are used to solve the non–LTE rate equations and to obtain new values for the departure coefficients for all depths. The new radiative rates and b_i's are used to update the run of the various ETLA parameters (see Mihalas 1978 for details) which are used in the next model iteration.

Having solved equation (3) for all wavelengths, we solve equation (7) and obtain a better estimate for the variation of the Lagrangian Eddington flux with optical depth. New geometry factors are calculated using the present values of J, H, and K (or the Euler system moments) and are updated at every model iteration. The updated function $H(\tau_{\rm std})$ is then used to solve equation (13) and compute the new temperature structure. The model iterations are stopped if the relative errors in the radiative equilibrium conditions and the temperature corrections, as well as the corrections for the b_i's, are less then 10^{-3}. We have checked the convergence properties of this scheme by using different initial estimates for the temperature structure and the run of the departure coefficients and found that the present scheme always leads to true convergence and avoids the very slow convergence of a Λ-iteration.

Typically, for a line-blanketed, non–LTE model atmosphere, we use $N_s = 50$ depth points logarithmically spaced between $\tau_{\rm std} = 10^{-6}$ and $\tau_{\rm std} = 10^4$, four angle points for the half-sphere distributed according to a Lobatto scheme (Abramowitz & Stegun 1965), and $\sim$1700 wavelength points from $\lambda = 20$ Å to $\lambda = 10^7$ Å. We have checked the effect of changing these code parameters on the structure of the atmosphere and the emergent spectrum and find these values sufficient for producing accurate results. For example, we also ran models with either eight angles per half-sphere or used an approximate Λ-

iteration method radiative transfer (Hauschildt 1992) and found no significant changes of the results. Depending upon the initial stratification, 10–15 iterations are required to satisfy both the energy conditions and the values of the departure coefficients to a relative accuracy better than 0.1%. The CPU times, required to fully converge a model atmosphere, range from ~4–6 hr on an IBM 3090-180 VF mainframe to ~6–9 hr on an IBM RS/6000-320 workstation. The code uses ~20 Megabytes of memory on either machine.

5. PROPERTIES OF NOVA PHOTOSPHERES

In this section we present the basic properties of the atmospheres that we have constructed to synthesize the observations of novae in the very earliest stages. In the next two sections we will compare our models to the observations. However, even before doing the comparisons it is possible to make some general statements about our model nova atmospheres based on the fact that the density exponent, n, in nova photospheres is ~2 ... 3 (Bath & Shaviv 1976; Starrfield 1989), as compared to $n \sim 5 \ldots 12$ for the envelopes of SN II. This difference has a number of important consequences:

1. Nova photospheres are far more geometrically extended than those of any other object known to us. Consequently, the curvature term in the transfer equation is of great importance in novae and radii determined from observations in different ways or wavelength regions can differ by large amounts (see Baschek, Scholz, & Wehrse 1991). We show this in Figure 7 by plotting the density at the outer boundary, r_{out}, as a function of the extension of the atmosphere (log r_{out}/R) and the reference radius, R, where the optical depth in scattering reaches unity (for $\lambda = 5000$ Å). This figure shows that for a given outer density the atmosphere becomes more extended as R decreases. Although we must point out that this statement is wavelength dependant. Note that the volume between r_{out} and R is accessible to spectroscopy since photons emitted at radius, R, can reach the observer. For all of our atmospheres, this volume is much larger than the opaque core region.

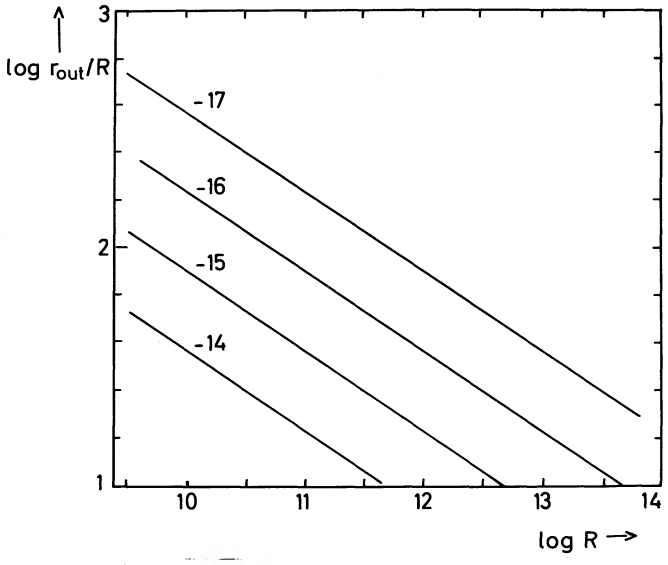

FIG. 7.—The relation between the outer radius r_{out} where the optical depth scale starts and the radius R where the optical depth in scattering is unity for different values of the density at r_{out}. The volume between r_{out} and R is directly accessible by spectroscopy since photons radiated from this region can reach the observer. It is seen that this volume is very much larger than the opaque core region.

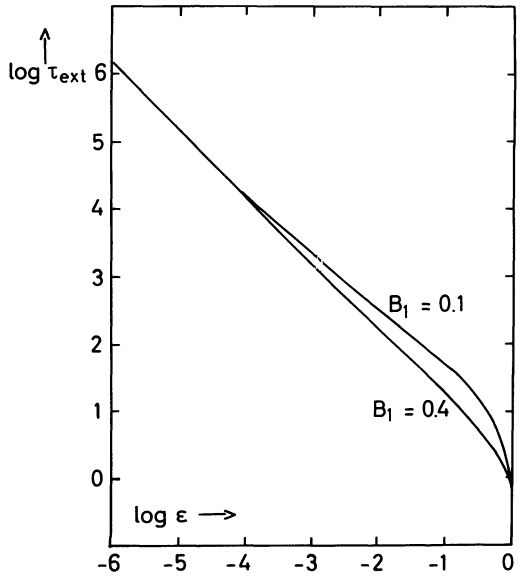

FIG. 8.—The optical depth in extinction where the local emissivity equals the emergent flux as a function of the ratio ϵ = absorption coefficient/extinction coefficient for two values of the gradient of the Planck function.

2. In the outermost layers the densities are so low that, in large parts of the atmosphere, electron scattering is the main source of opacity and photons generated from thermal emission at rather large depths, in the expanding layers, can reach the surface (possibly, after a number of scatterings). In order to demonstrate this effect we have used the radiative transfer code to calculate the radiation field inside a plane-parallel atmosphere with constant ϵ (where ϵ = absorption coefficient/extinction coefficient) and a linear Planck function $B_\lambda(\tau)[B_\lambda(\tau) = B_0 + B_1\tau]$. We then determined the optical depth, τ^0_{ext}, at the point where the emergent flux equals twice the local emissivity (the factor of 2 comes from the angle integration). The results (see Fig. 8) show that τ^0_{ext} may, in fact, become very large when ϵ becomes very small. Therefore, if ϵ is small, photons can arise from very deep layers where the temperature is high. Note, however, that for pure absorbing atmospheres τ^0_{ext} is always equal to $\frac{2}{3}$, independent of the value of B_1. These results imply that *the color temperatures of scattering dominated, extended atmospheres can be very high.* This is shown in Figure 9 in which we plot the optical depth in absorption, where the local emissivity equals the emergent flux, as a function of ϵ. Note that the vertical axis is not logarithmic as in Figure 8 but linear.

3. The mass depth into the atmosphere, $M_{visible}$, from which photons can escape (that part of the atmosphere directly visible to an outside observer), may be rather large. In Figure 10 we plot the mass, $M_{visible}$, visible to an observer for two values of the outer density. The full curves refer to an optical depth in scattering of unity, i.e., the volume between r_{out} and R, and the broken curves indicate masses up to a scattering optical depth of 300 ($\approx$ the maximum optical depth from where a photon can emerge without absorption). As is seen in Figure 10, $M_{visible}$ can reach an appreciable fraction of the total accreted mass of $\sim 10^{-6}\ M_\odot$ to $\sim 10^{-5}\ M_\odot$ (Starrfield 1989; Shara 1989). As the expanding atmosphere evolves with time, $M_{visible}$

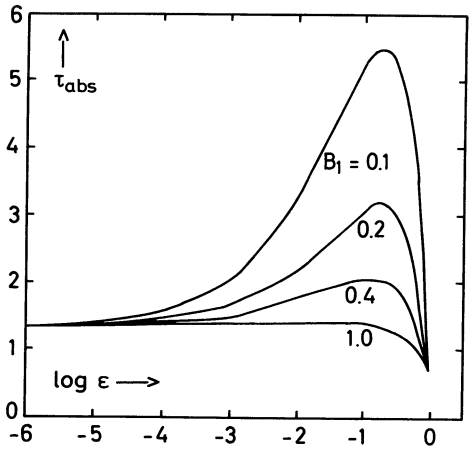

FIG. 9.—The optical depth in absorption where the local emissivity equals the emergent flux as a function of ϵ. Note that the vertical axis is not logarithmic as in Fig. 8 but linear.

increases and, therefore, the extremely hot deeper layers become visible in later phases.

4. The temperature distributions are characterized by optically thin (in absorption) outer parts in which the temperature $T \propto r^{-1/2}$ (as a consequence of geometric dilution) and inner parts where the temperatures rise very fast. We show this in Figure 11 where we plot the temperature distributions in nova photospheres for our model atmospheres with $R_{(\tau_{abs}=1)} = 10^{11}$ cm, outer densities $\rho_{out} = 2 \times 10^{-15}$ g cm^{-3} and effective temperatures, $T_{eff} = 10^4$, 1.5×10^4, and 2×10^4 K. Also plotted are the corresponding plane-parallel, gray distributions (dotted curves). These plots show that the ionization conditions can vary extremely widely in nova photospheres and that one should observe a large number of ionization stages simultaneously present in the spectrum. *We emphasize that the observations of multiple ionization stages in novae spectra is one of the important diagnostics of these spectra and its cause has been, heretofore, unexplained.* In addition, for some of our model atmospheres, the outer temperature is low enough, so that molecules and perhaps even dust can form in the outer layers as is observed (see, for example, Gehrz 1988).

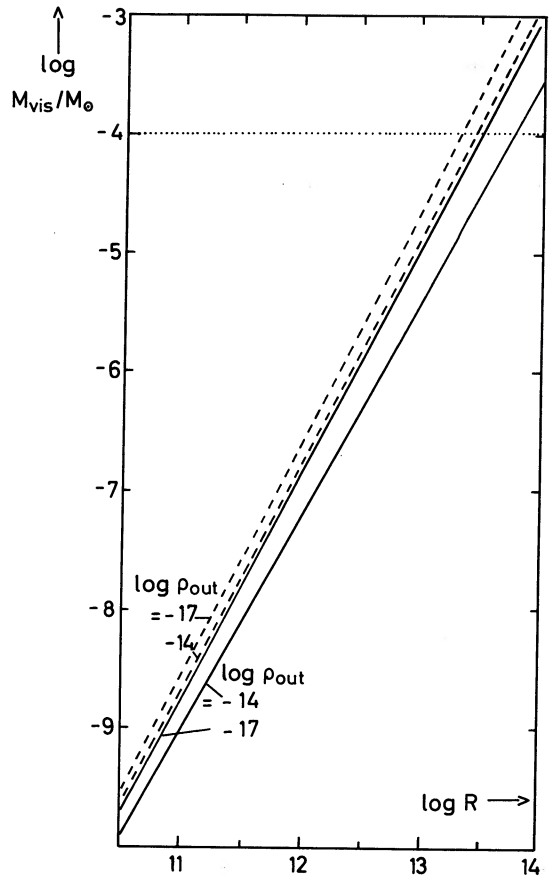

FIG. 10.—The mass $M_{visible}$ visible to an observer for two values of the outer density. The full curves refer to an optical depth in scattering of unity, i.e., the volume between r_{out} and R, and the broken curves indicate masses up to the scattering optical depth 300 ($\approx$ the maximum optical depth from where a photon can emerge without absorption).

5. An appreciable part of the matter receding from the observer (i.e., matter which is on the "backside") can actually be seen in the quite extended red wings of strong lines.

6. While the non–LTE effects on the temperature structure

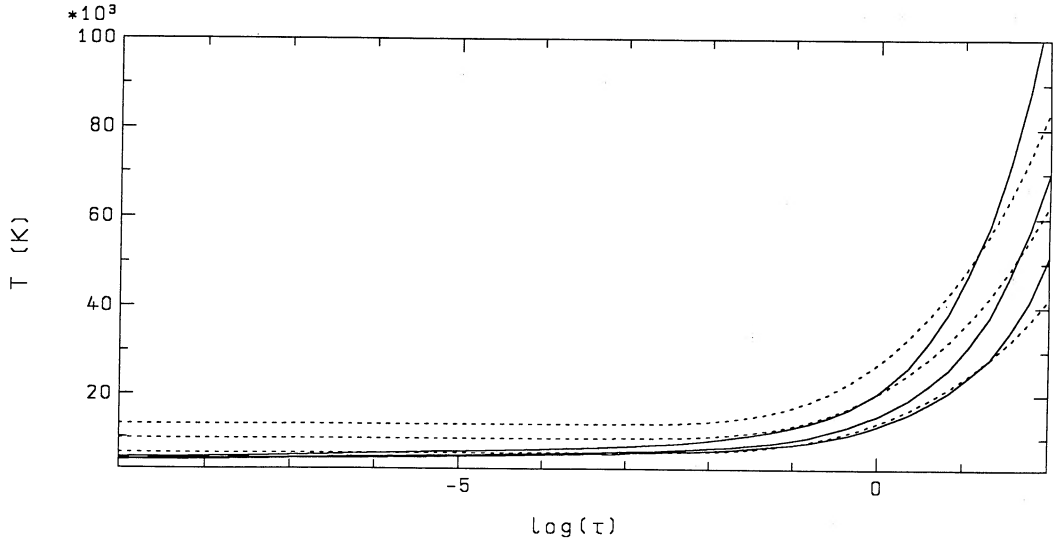

FIG. 11.—The temperature distributions in nova photospheres with $R_{(\tau_{abs}=1)} = 10^{11}$ cm, outer densities $\rho_{out} = 2 \times 10^{-15}$ g cm^{-3} and effective temperatures $T_{eff} = 10^4$, 1.5×10^4, and 2×10^4 K. Also plotted are the corresponding gray distributions (*dotted curves*).

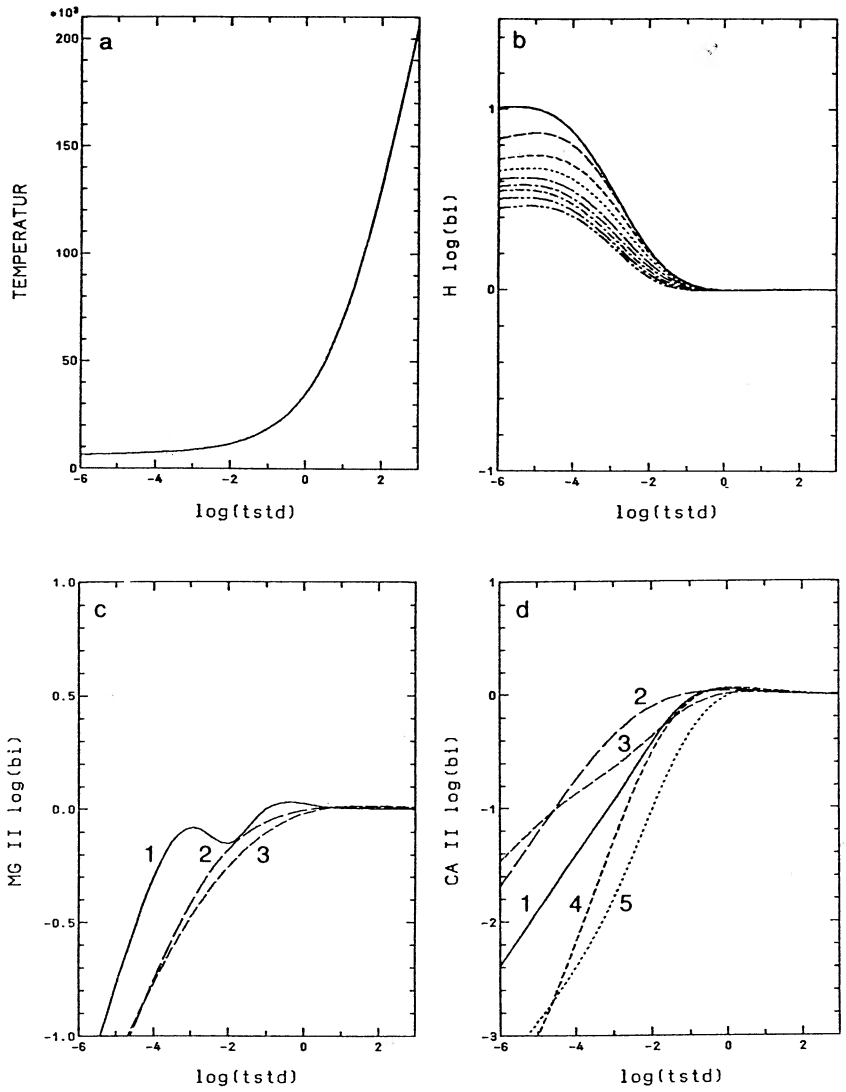

FIG. 12.—Temperature structure (*a*) and variation of the departure coefficients for H I (*b*), Mg II (*c*), and Ca II (*d*) vs. τ_{std}. The curves in (*b*)–(*d*) are labeled by the level number.

are quite small, the departure coefficients differ from unity in the line forming regions of the photosphere. In order to demonstrate this effect, we show in Figure 12 the temperature structure and the variation of the departure coefficients with optical depth for a model with $T_{\rm eff} = 25{,}000$ K, $L = 2 \times 10^4$ $L_\odot$, and $v_{\rm max} = 2000$ km s^{-1}. The deviations from LTE are large in the outer parts of the atmosphere and will have a large influence on the profiles of strong lines such as Mg II $h + k$. Nevertheless, the temperature structure is dominated by the effects of the UV lines on the radiative equilibrium condition, so that the temperature differences between the LTE and non–LTE models are very small.

7. The effects of line blanketing on the spectra are very large, in particular for the cooler models ($T_{\rm eff} \leq 25{,}000$ K). This is due to the "Fe II forest" which forms a quasi-continuum in the UV range. Therefore, the color temperatures, derived from the UV spectra, of our cooler model atmospheres are much lower than the effective temperature as defined above. This result indicates that blackbody fits to observed spectra can lead to large errors in the temperatures. In the hotter models, Fe II is ionized to Fe III, even in the outermost parts of the atmosphere, so that the total extinction in the UV wavelengths is much smaller.

8. Finally, in Figure 13 we demonstrate one of the most important results of our calculations by showing the effects of enhanced CNO abundances on the spectral energy distributions. For an atmosphere with $T_{\rm eff} = 2 \times 10^4$ K, $L = 2 \times 10^4$ $L_\odot$, and $v_{\rm max} = 2000$ km s^{-1}, the general effect is to increase the absorption at (some) UV wavelengths ≤ 1600 Å. In this region, most of the features are due to weak CNO lines. Three different calculations are presented in Figure 13: solar CNO abundances (solid line), 10 times solar CNO abundances (dashed line), and 100 times solar CNO abundances (dotted line). Note that the flux scale is logarithmic. The effects of abundance variations are located in relatively small regions of the spectrum (the regions where most of the lines are weak CNO lines). We do not expect, for this choice of parameters, larger differences in the general shape of the spectrum since line blanketing dominates continuum absorption and the CNO continuum edges will not be visible in the spectrum. The effect

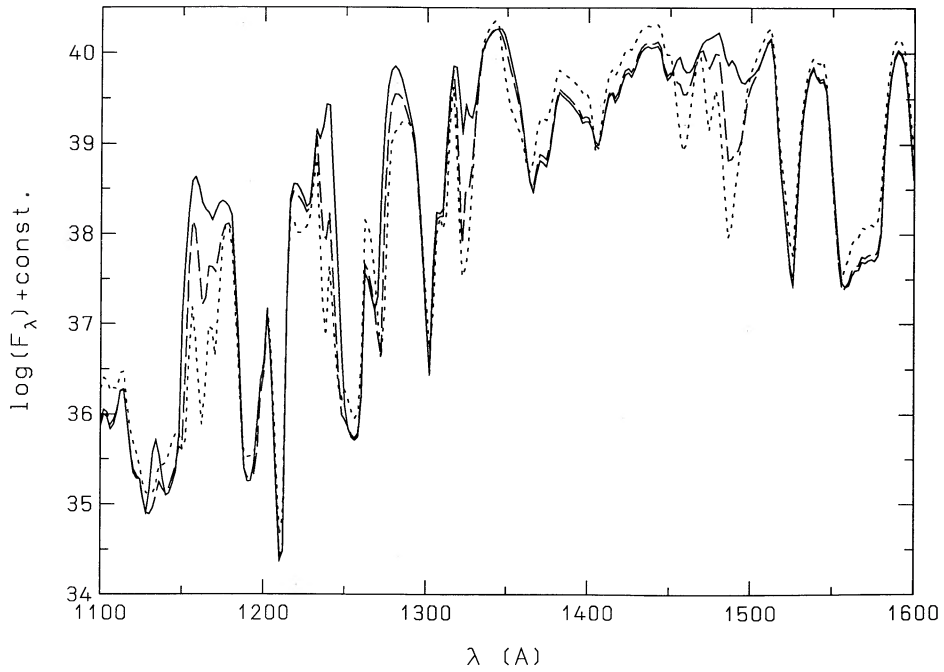

FIG. 13.—Effects of increased CNO abundances on the UV spectrum of model N25. The logarithm of the emergent flux is plotted vs. wavelength in angstroms. The solid curve gives the spectrum of model N25 calculated with solar abundances, the dashed line the spectrum of model N25 with 10 times solar CNO abundances and the dotted curve gives the spectrum of model N25 calculated with 100 times solar CNO abundances. All models were iterated to convergence with their respective abundances.

of abundance variations on the continuum edges are seen only in our test models in which line blanketing was not included. However, for atmospheres with larger $T_{\rm eff}$, we expect significant effects on the continuum since line blanketing in this spectral region is less important.

6. THE SYNTHETIC SPECTRA

Our calculations have now reached the stage where we feel confident in comparing our synthetic spectra, derived from the model atmospheres, with the *IUE* observations shown in § 2. In order to explain some of the features of the observations, in Figures 14 and 15 we show the energy distributions for LTE models in which only continuous absorption and scattering have been taken into account. These atmospheres have $T_{\rm eff} = 10^4$ K, 1.5×10^4 K, and 2×10^4 K, $R_{(\tau_{\rm abs}=1)} = 10^{11}$ cm, $\rho_{\rm out} = 2 \times 10^{-15}$ g cm^{-3}, and $M = 10^{-7}\ M_\odot$ yr^{-1} leading to a maximum expansion velocity of $v = 10^3$ km s^{-1}. We assume a solar composition for the CNO nuclei. While we are fully aware that nova abundances can be far from solar, we regard these calculations as our baseline study to which further work will be compared.

In Figure 14 we show continuum fluxes for model nova photospheres (solid curves) with $R_{(\tau_{\rm abs}=1)} = 10^{11}$ cm, outer densities $\rho_{\rm out} = 2 \times 10^{-15}$ g cm^{-3} and effective temperatures

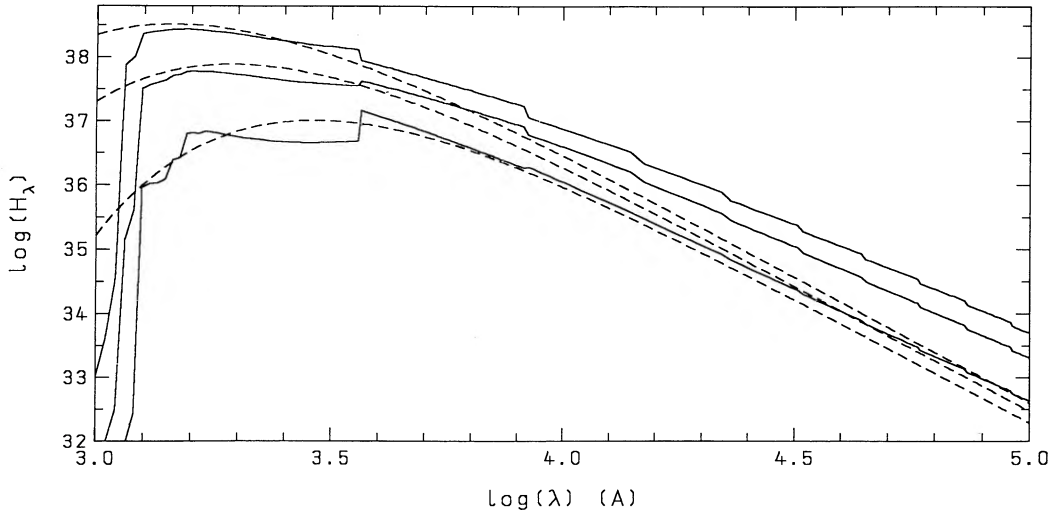

FIG. 14.—Continuum fluxes of nova photospheres (*solid curves*) with $R_{(\tau_{\rm abs}=1)} = 10^{11}$ cm, outer densities $\rho_{\rm out} = 2 \times 10^{-15}$ g cm^{-3} and effective temperatures $T_{\rm eff} = 10^4$, 1.5×10^4, and 2×10^4 K from the ultraviolet to the infrared range. The broken lines give blackbody fluxes for the same temperatures.

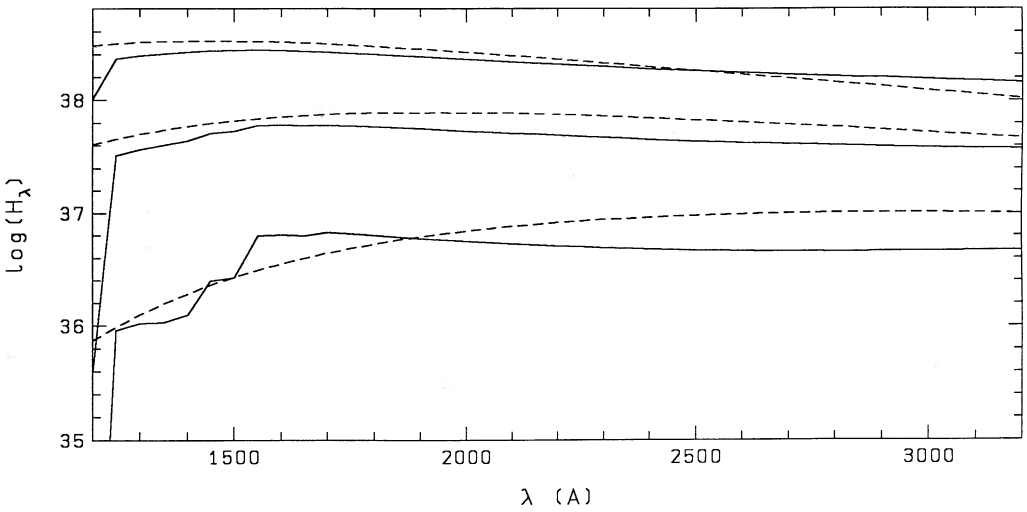

FIG. 15.—Same as Fig. 14 but on an extended linear scale for the UV wavelength range.

$T_{\rm eff} = 10^4$, 1.5×10^4, and 2×10^4 K, from the ultraviolet to the infrared range. In Figure 15 we show the same atmospheres but here we have only plotted the spectral region covered by the *IUE* satellite. In both plots, the broken lines are the blackbody fluxes for the same temperatures. It can be seen that, at infrared wavelengths, our atmospheres have both a strong excess over an equivalent blackbody distribution and, in addition, exhibit a very flat energy distribution which is caused by the large atmospheric extension discussed earlier. We see that color temperatures taken from observed energy distributions *cannot* be interpreted as direct evidence for the existence of material with the corresponding temperature in the atmosphere. The Paschen and Balmer jumps in these models are both quite weak and, in addition, can be either in emission or absorption as was shown earlier by Harkness (1983). The cause of this behavior is that the flux per unit surface area on the short wavelength side of the jump is smaller than that on the long wavelength side (since it is formed in the outer and cooler layers). However, this effect may be partially compensated for, or even overcompensated for, by the larger emitting area. The Lyman edge is always in absorption because the steep gradient of the Planck function with respect to the temperature, for wavelengths below 912 Å, always prevails over the extension of the atmosphere. In the UV, the absorption edges of some neutral species (C I, Mg I, Si I, etc.) are present even for atmospheres with very high $T_{\rm eff}$. This is caused by the presence of these species in the outer, cooler, layers. In the inner parts of the atmospheres, the radiation field at these frequencies is very high.

Figure 16 shows the effects of blanketing on our model atmospheres. The atmosphere shown in this graph has a radius $R_{(\tau_{\rm abs}=1)} = 10^{11}$ cm, an outer density $\rho_{\rm out} = 2 \times 10^{-15}$ g cm^{-3}, and an effective temperature $T_{\rm eff} = 10^4$ K. The three curves show the fluxes of a continuum model (dashed line), a metal line-blanketed model with only the strongest lines included (solid line), and a blackbody (dotted line) with the same $T_{\rm eff}$. All lines appear to be in absorption since the Planck function drops off rapidly (which can also be deduced from the very small residual fluxes). Although, in this paper, we did not check the contributions of specific transitions, it seems to us that essentially all observed features found in the early UV spectra of novae, obtained with the *IUE* Satellite, are severe blends. Finally, the line profiles for novae spectra are quite narrow as compared to those for supernovae spectra since the spread of expansion velocities within the atmosphere is much smaller. However, they are much broader than found in normal hydrostatic stars with the same $T_{\rm eff}$.

7. MODELS FOR PW VUL

We now proceed by showing a series of plots which compare our non–LTE model atmospheres to some of the observed spectra of PW Vul given in § 2. Since Saizar et al. (1991) obtained nearly solar abundances for the CNO nuclei from an analysis of the nebular lines of PW Vul, we have also begun with solar abundances in our model atmosphere calculations. Using the methods outlined in the previous sections, we have calculated models with the parameters given in Table 1. All our models have a luminosity of $L = 2 \times 10^4\ L_\odot$, $n = 3$, and a maximum expansion velocity of 2×10^3 km s^{-1}. In both the model construction and the computation of the synthetic spectra, we have assumed a statistical (microturbulent) velocity of $\zeta = 300$ km s^{-1}. The model parameters were taken from hydrodynamic calculations and no attempt was made, at this stage of the analysis, to fine-tune the parameters in order to achieve a better fit to the observations. This will be done in a later paper. In this paper we concentrate on introducing the method and describing the basic comparison of our atmospheres with the observations.

In Figures 17*a* and 17*b* we again show the *IUE* spectrum of PW Vul obtained on 1984 August 5. The dashed line gives the synthetic spectrum obtained from model N10. Although the region between 2800 and 3150 Å is overexposed, the *relative* run of the observed spectrum should be fairly accurate. As can be seen from Figure 17, the model is able to reproduce most of

TABLE 1

MODELS FOR PW VUL

Model	L ($L_\odot$)	$T_{\rm eff}$ (K)	R_0 (cm)	$\dot{M}$ ($M_\odot$ yr^{-1})	n
N10.....	20×10^3	10,000	3.28×10^{12}	2.8×10^{-4}	3
N25.....	20×10^3	25,000	5.24×10^{11}	1.8×10^{-5}	3
N30.....	20×10^3	30,000	3.64×10^{11}	1.1×10^{-5}	3

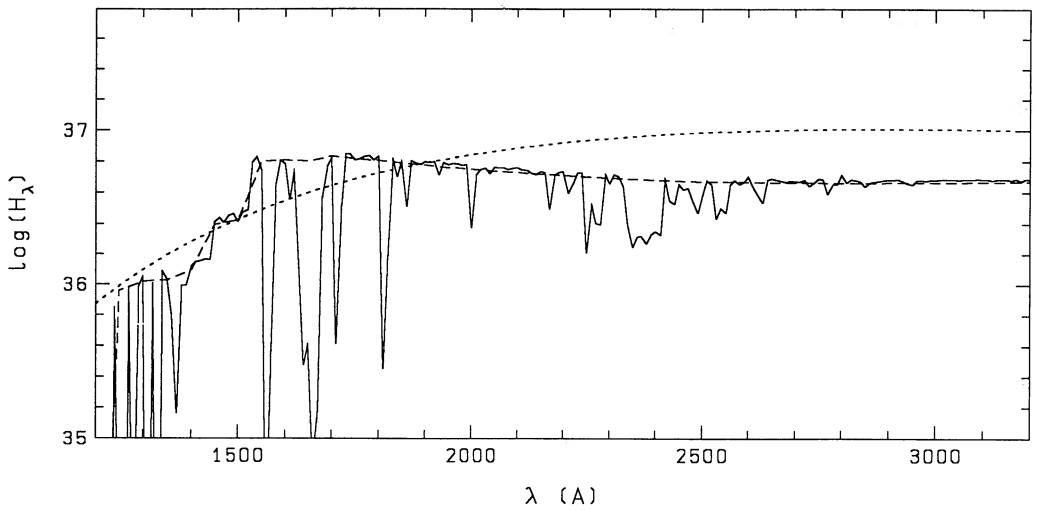

FIG. 16.—Comparison of the fluxes of a continuum model (*dashed curve*) which has a radius $R_{(\tau_{abs}=1)} = 10^{11}$ cm, outer density $\rho_{out} = 2 \times 10^{-15}$ g cm^{-3}, and $T_{eff} = 10^4$ K, with metal line-blanketed model (with the same parameters) that includes only the strongest lines (*solid curve*). We also plot a blackbody (*dotted line*) with the same temperature.

the observed features. In particular, the P Cygni profile of the Mg II $h + k$ lines at 2800 Å is seen both in the model and the *IUE* spectrum. The differences between the observed and the synthetic spectrum in the SWP range could be due to either the model parameters (the LWP range for $T_{eff} = 10^4$ K is in the Wien part of the spectrum) or variations in the abundances. However, no effort has been made at this stage to obtain a better fit by changing the model parameters.

The *IUE* spectrum obtained on 1984 September 30 looks very different from the previous spectrum. In Figures 18*a* and 18*b* we show the LWP and SWP spectra compared with synthetic spectra obtained from the models N25 and N30. The SWP range is fairly well reproduced by both models. The run of the continuum is better represented by model N30 but some lines seem to be better fitted by model N25. The fit is better in the LWR range and model N25 seems to fit the continuum and lines somewhat better. Unfortunately, the region around the Mg II $h + k$ lines is badly overexposed so that we cannot make specific statements about these lines from the low-resolution spectra. However, a comparison of the model spectra with LWP high-resolution spectra of PW Vul, obtained early in the outburst, does show good agreement between the models and the observed line profiles of Mg II $h + k$. It seems that in both models the lines are broader than observed, which could be attributed to a smaller value of the statistical velocity ζ. Although most lines in the models appear with the observed red- or blueshift, there are lines in the synthetic spectrum which have too large or too small a red- or blueshift as compared to the observed spectrum. This could be explained by a change in the exponent n in the density law because the lines form in different parts of the atmosphere and consequently have different red- or blueshifts due to large-scale velocity fields. It seems, therefore, that it will be possible to obtain an accurate value of n by comparing the relative wavelength shift of lines from different regions in the expanding atmosphere and provide both constraints on the hydrodynamic simulations and information on the ejection mechanisms.

On 1984 November 13 the observed *IUE* spectrum looks similar to that of September 30. In Figures 19*a* and 19*b* we compare the observed spectra with models N25 (dotted curve) and N30 (dashed curve). In general, we get very similar results from the fit shown for September 30. However, now the line spectrum from model N25 fits the feature at ~3000 Å quite well, although the emission peak is somewhat overexposed. Unfortunately, the region of the Mg II $h + k$ lines is still overexposed as in the previous spectra. The slope of the continuum is reproduced by both models. We suggest that the effective temperature of PW Vul on 1984 November 13 must lie in the range from 25,000 to 30,000 K.

In order to demonstrate the effects of composition changes on the spectra, we have calculated an additional model in which the abundances of heavy elements was increased by 0.7 dex. Figure 20 shows that the overall structure of the spectrum remains unchanged.

However, individual lines can appreciably change their strengths and shapes due to the very complex competition between the temperature gradient and the atmospheric extension. This causes some lines to go into emission. It is important to realize that changing the elemental abundances severely affects the lines and that it will be relatively straightforward to obtain abundances from analyses of observed spectra using models such as we have presented in this paper.

In order to investigate possible consequence of deviations from radiative equilibrium, we calculated, in addition, an LTE model in which the temperature for layers with $\tau_{abs} < 10^{-4}$, was kept (artificially) constant. As is seen in Figure 21, the line spectrum changes dramatically. There is a significant change in the shapes and strengths of many features and some go strongly into emission although the relative change in the total flux is $\sim 10^{-3}$. This result implies that the occurrence of emission lines in observed spectra indicates either that the continuum has become weak (i.e., the continuum is formed deep inside the line formation region) or that the temperature in the outer regions is enhanced by the dissipation of nonradiative energy. We hope that further modeling will allow us to derive the relative importance of these effects from the flux ratios.

We emphasize that the model atmospheres that we have presented here show that it will be possible to make quantitative interpretations of early novae spectra. We are continuing this work with an extensive program to compare observed and theoretical spectra. However, it is also evident that to obtain the full accuracy in the comparisons it will be necessary to

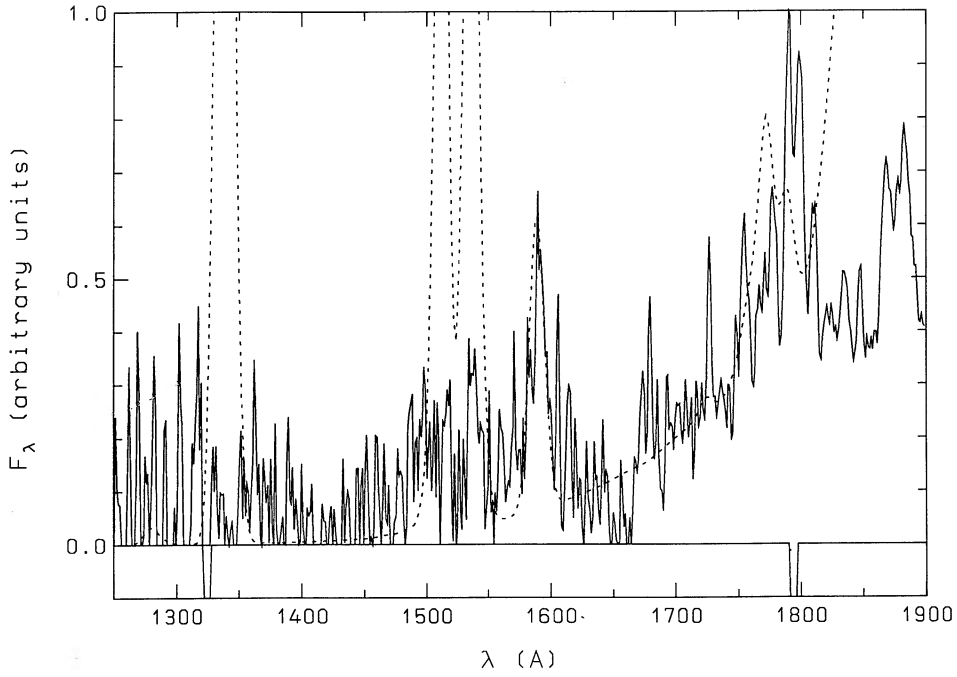

FIG. 17*a*

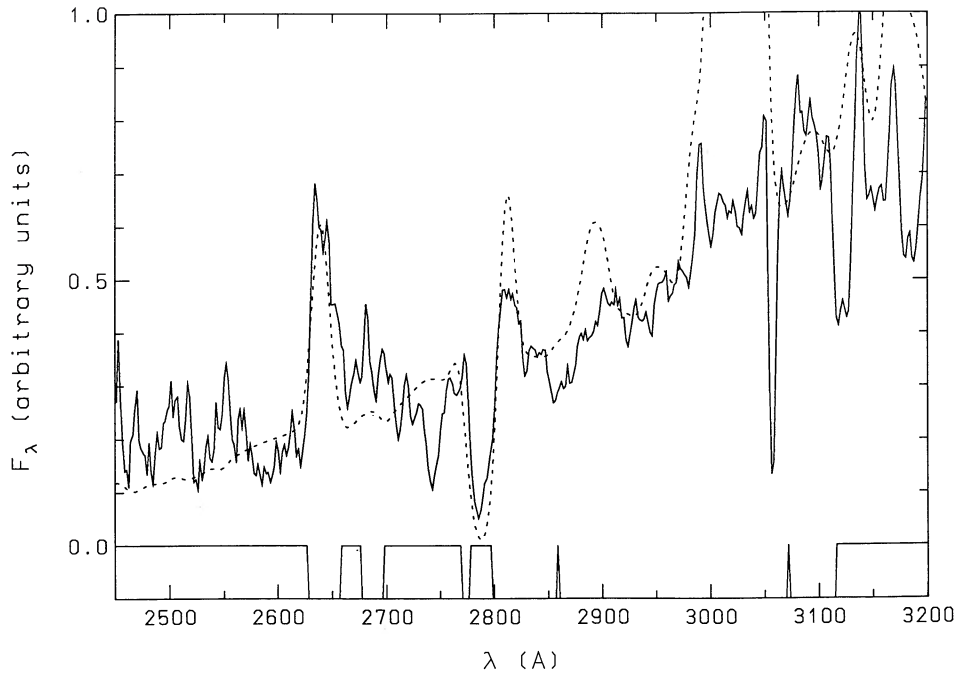

FIG. 17*b*

FIG. 17.—(*a*) SWP and (*b*) LWP spectra of PW Vul on 1984 August 5 compared with the model N10 (*dashed lines*). The relative flux is given on a linear scale. Overexposed parts of the *IUE* spectra are indicated by negative values of ϵ (see § 2).

incorporate a full non–LTE treatment of ions like He I, He II, C II, C III, N II, N III, Fe II, Fe III, and others into the solutions. Inclusion of these ions will improve the accuracy of the abundances derived from subordinate transitions and from lines which are formed very close to the top of the expanding layers.

Another problem, which must eventually be resolved, is that spatially resolved images of nova envelopes often show significant deviations from spherical symmetry so that two- or even three-dimensional modeling of the density, temperature, and radiation fields will be required. Such modeling is feasible using present day computers (see, for example, Stenholm, Störzer, & Wehrse 1989). In addition, both direct images and high-resolution spectra (Krautter et al. 1984) demonstrate that nova shells are not homogeneous, as is assumed in the models, but that, instead, they possess inhomogeneities (knots, blobs, etc.) of very different scales and contrasts. Therefore, a sta-

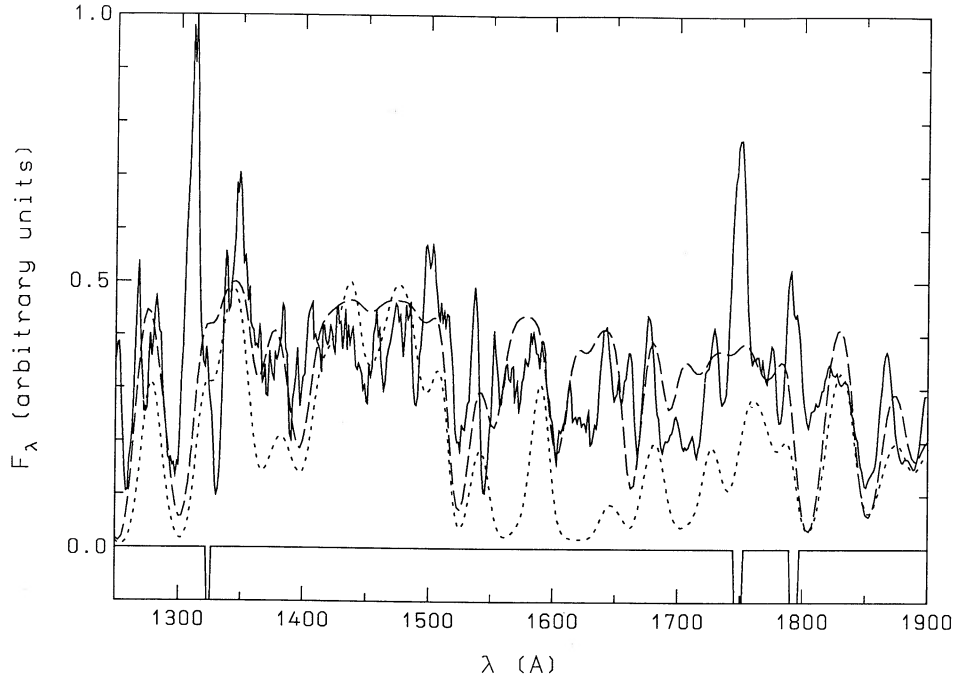

FIG. 18*a*

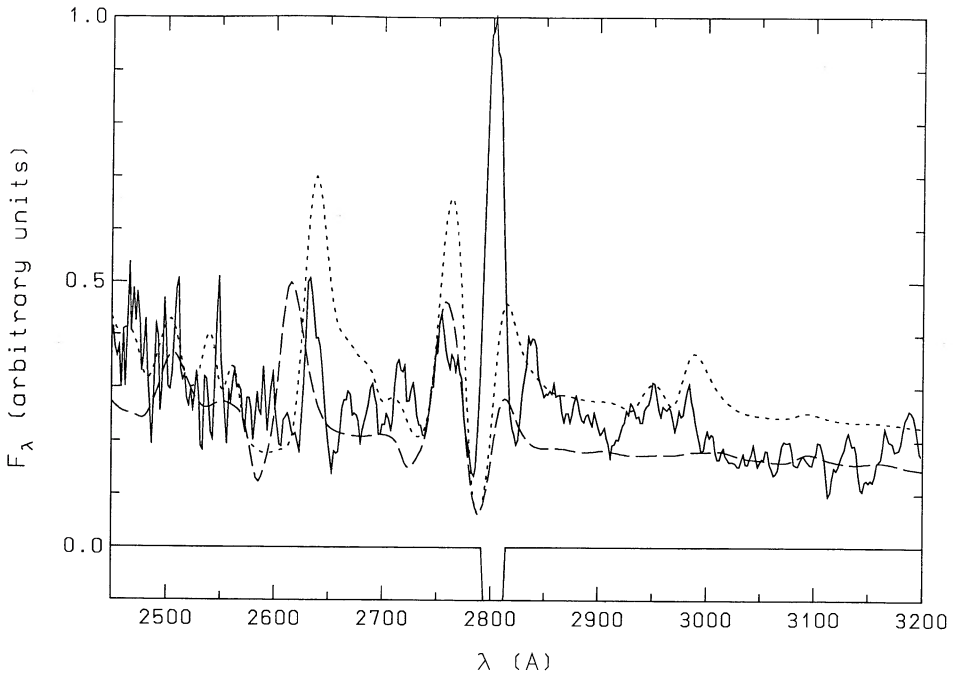

FIG. 18*b*

FIG. 18.—(*a–b*) Same as for Figs. 17*a* and 17*b*, but for 1984 September 30. The long-dashed line shows the theoretical flux from model N30, while the dotted line is the flux from model N25.

tistical treatment of the atmospheres would be more appropriate. A straightforward generalization of our approach, utilizing the method developed by Gierens et al. (1986), should not only give a better representation of reality but, in addition, it should be possible both to unravel the information contained in the local minima and maxima of line profiles and also to obtain improved estimates of the errors in the derived parameters.

8. SUMMARY AND DISCUSSION

In this paper we have reported on the development and utilization of a new non–LTE, line blanketed, spherical, expanding, model stellar atmosphere computer program. Atmospheres calculated with this program have been compared to UV spectra obtained from the *IUE* satellite archives.

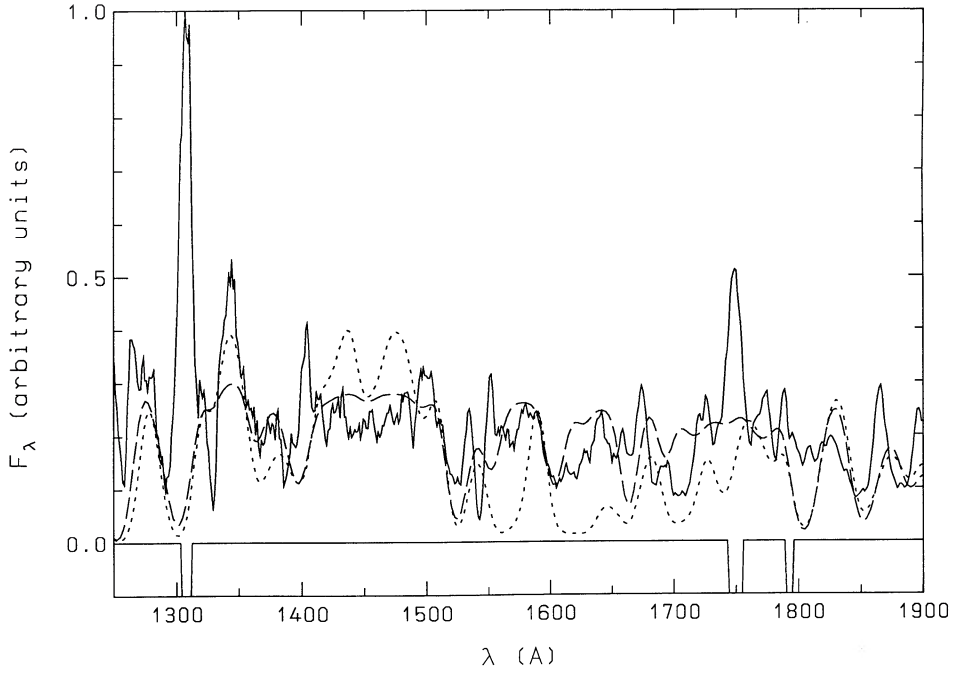

FIG. 19*a*

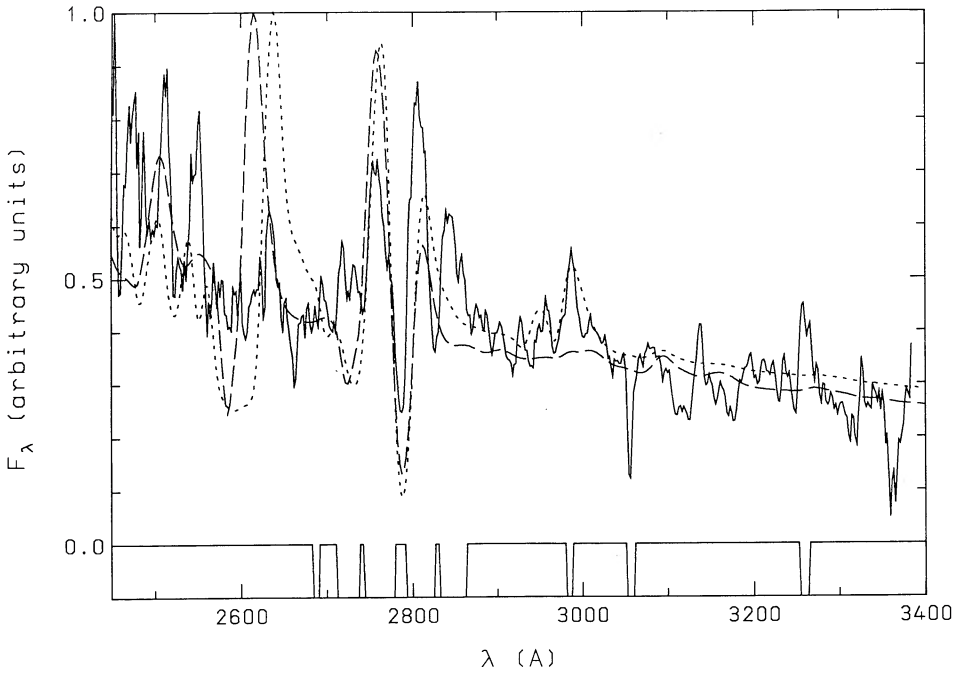

FIG. 19*b*

FIG. 19.—(*a*–*b*) Same as for Figs. 17*a* and 17*b*, but for 1984 November 13. The long-dashed line is the theoretical flux obtained from model N30, while the dotted line is the flux from model N25.

The comparisons are quite good and demonstrate the power of new methods in model atmosphere theory for analyzing stellar spectra. We note, however, that the spectra presented here have been calculated using the assumptions of radiative equilibrium and solar composition which are questionable for novae. For example, during the explosion it seems reasonable that shocks can form and heat the outer layers by non-radiative processes. It is also likely that the material ejected from off of the white dwarf will impact either the accretion disk, the secondary star in the system, or both, producing not only shock heating but, in addition, entraining some of this additional material in the outgoing flow.

It is also clear that most novae show strong evidence for enhanced abundances of the CNONeMg elements (Truran &

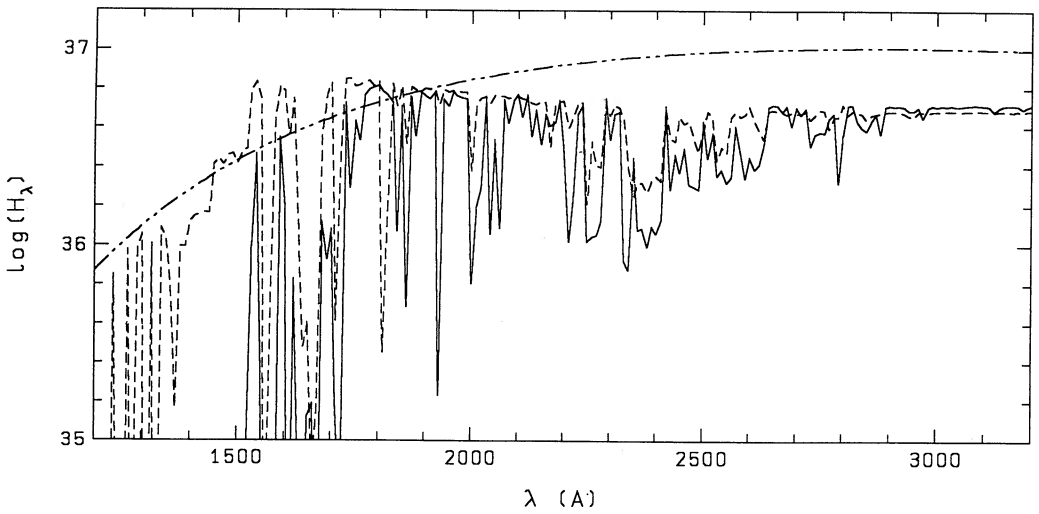

FIG. 20.—Effects of abundance changes on the UV spectra of novae: the dashed curve shows the same blanketed flux distribution as Fig. 16, whereas for the solid curve an overabundance of all heavy elements by a factor of 5 is assumed. The dotted line is the blackbody spectrum.

Livio 1986; Starrfield 1989; Sparks et al. 1988) and we have used primarily solar abundances in this study. Nevertheless, we regard this paper as the beginning of a series of analyses of the nova spectra that exist in the *IUE* archives and those novae must cover a very broad range in abundances.

One of the important studies in this paper has been to examine the effects of small values of n, the exponent in the density law, on the structure of the atmospheres. Hydrodynamic simulations have shown that n should have values around 2–3 in novae, values much smaller than those expected for supernovae expansions of ~ 5 to 13. The small value of n results in nova photospheres that are very extended as compared to those of supernovae so that the curvature term is of great importance and radii determined at different wavelengths can be very different. We have also found that the densities become so low that electron scattering is the principal source of opacity and photons generated at very large depths in the expanding material can reach the surface. In fact, in some cases the photons can escape from mass depths into the atmosphere which are sizable fractions of the entire ejected envelope. One interesting and observable prediction, is that these atmospheres exhibit excess emission over an equivalent blackbody distribution at infrared wavelengths.

Since at some wavelengths one can see very deeply into nova photospheres, even near maximum light, the observer is sampling material at very different temperatures. Thus, the ionization conditions will vary widely and a large number of ionization stages of the same element should be simultaneously present in nova spectra. This is observed and has been unexplained until now. This result will turn out to be an important diagnostic of nova photospheres. For some of our model atmospheres, the outermost temperatures can become so low that molecules can form. In fact, this prediction is currently being tested in an investigation of molecule and grain formation in nova envelopes.

Because of the interrelationship between the hydrodynamic simulations and our atmospheres, we also calculate the integrated opacities from our models (flux mean, Planck mean,

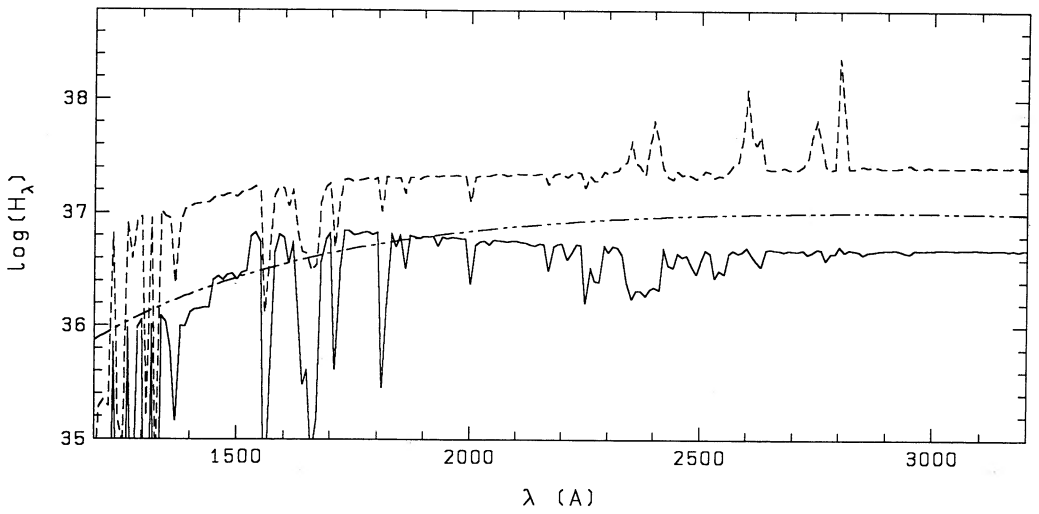

FIG. 21.—Demonstration of the significance of the temperature distribution in the outer layers: the solid curve shows the same blanketed energy distribution as Fig. 16 for which the temperature distribution of Fig. 11 is used for all optical depth whereas for the broken curve it is assumed that the temperature distribution follows this run only up to $\tau_{abs} < 10^{-4}$ and is constant for the upper layers.

Rosseland mean) and will provide them to the hydrodynamic studies in order to improve their results.

We have also investigated the effects of line blanketing on the structure of our atmospheres and found, as expected, that it is very large. For our cooler models ($T_{\rm eff} \leq 25{,}000$ K, the Fe II "forest" forms a quasi-continuum at UV wavelengths. This implies that the temperatures derived from UV spectra can differ appreciably from the actual $T_{\rm eff}$ and blackbody fits to the observed energy distribution can lead to large errors in the temperature. This result explains not only why the observed continua of "early" nova spectra show a steep rise to the red but, in addition, why most of the "emission" lines have remained unidentified. *They are not actually emission lines but regions of transparency between overlapping absorption from the* Fe II *forest.*

We have briefly (more extensive comparisons will be shown in later papers in this series) studied the effects of enhanced abundances on the emergent spectrum. The general effects of increasing the abundances of the CNO nuclei is to increase the absorption at some wavelengths in the region from $\sim$1220 Å to $\sim$1600 Å. There are noticeable changes in the emitted line spectrum increasing our confidence that we will be able to determine the ejecta abundances for those novae with spectra in the *IUE* archives.

We showed some of the spectra of CO novae in the *IUE* archives in order to demonstrate the excellent fit between our model atmospheres and the observations. Nevertheless, even a cursory comparison between the early spectra of CO novae and fast ONeMg novae show major differences. We attribute these differences to the fact that the fastest CO novae eject more material than the fastest ONeMg novae; a result that must be interpreted by the hydrodynamic simulations. One of our primary goals is to analyze the early spectra of fast ONeMg novae and try to verify this hypothesis. This will require the extension of our atmospheres to much hotter effective temperatures.

Finally, we note that our models require the luminosity and effective temperature of the nova in order to fit the theoretical spectrum to the observed spectrum. By performing our fits to spectra obtained over broad time ranges in the evolution of the novae we will be able to not only improve our knowledge of the energy emitted during the outburst but, in addition, to constrain the hydrodynamic modeling of the outbursts and the distances to the novae. This will be especially important for the observations of novae in the LMC. If HST is able to obtain UV spectra of novae in M31, then our results could improve the distance estimates to these novae.

We are very grateful to J. Krautter, S. Shore, G. Sonneborn, W. M. Sparks, J. Truran, and R. M. Wagner for discussions about novae and their spectra. We are grateful to M. Shara for his thoughtful comments on an earlier draft of this paper. S. S. is grateful to S. Colgate, A. N. Cox, C. F. Keller, M. Henderson, and K. Meyer for the hospitality of the Los Alamos National Laboratory and a generous allotment of computer time. P. H. H. and R. W. thank the Department of Physics at Arizona State University for their hospitality during several visits. This work was supported in part by NSF Grants AST85-16173 and AST88-18215 to Arizona State University, by the Institute of Geophysics and Planetary Physics at Los Alamos, by NASA grants to Arizona State University (NAG5-481 and NAGW-2628) and to the University of Colorado (NAS5-28731), and by the DOE. G. S. thanks the VP fund for the promotion of research at the Technion.

APPENDIX

For the determination of the radiation field we subdivide the atmosphere into N_s shells and we first solve the transfer equation for each of these shells separately. Since the pressure and the temperature do not vary much in a given shell we assume that within each of them the ratio of scattering to extinction is independent of the depth. If we discretize the angle space, the radiative transfer equation (3) transforms from an integro-differential equation into a system of differential equations with constant coefficients. It has to be solved as an initial value problem with respect to the wavelength derivatives and as a boundary value problem with respect to the radial derivatives. If we now discretize the wavelength space we obtain a coupled system of ordinary differential equations which can be solved recursively for one wavelength grid point after the other. We write such a system for shell i ($i = 1 \ldots N_s$) in matrix notation

$$\frac{\partial \boldsymbol{I}_l}{\partial \tau} = \boldsymbol{A}_l \boldsymbol{I}_l + \boldsymbol{\Psi}_l \boldsymbol{B}_l + \boldsymbol{\Phi}_l \boldsymbol{I}_{l-1} , \tag{A1}$$

where the intensity vector $\boldsymbol{I}_l$ consists of the specific intensities for all angles at wavelength λ_l and optical depth τ, where l is the wavelength index. The $\boldsymbol{A}_l$ matrix contains the coupling coefficients for the specific intensities at the wavelength under consideration, the $\boldsymbol{\Psi}_l$ matrix describes the weighting coefficients for the Planck function, the vector $\boldsymbol{B}_l$ contains the Planck function at both r_i and r_{i-1} and finally the vector $\boldsymbol{\Phi}_l \boldsymbol{I}_{l-1}$ comprises the contributions from the previous wavelength which have "source character," i.e., which are proportional to the specific intensity at the previous wavelength grid point λ_{l-1} and contribute directly to the radiation field at the given wavelength λ_l. The solution of equation (A1) for shell i is given in terms of the matrix exponential function by

$$\boldsymbol{I}_\lambda(r_i) = \exp\,(\boldsymbol{A}_l \Delta\tau)\left\{\boldsymbol{I}_l(r_{i-1}) + \int_0^{\Delta\tau} \exp\,(-\boldsymbol{A}_l s)\boldsymbol{\Psi}_l \boldsymbol{B}_l(s) + \boldsymbol{\Phi}_l \boldsymbol{I}_{l-1}(s)]ds\right\} , \tag{A2}$$

with $\Delta\tau$ being the optical thickness of the shell at wavelength λ_l. Since the ingoing intensities at r_{i-1} and the outgoing intensities at r_i are given as boundary values we have to split all expressions accordingly and have to solve for the outgoing intensities $\boldsymbol{I}^+$ at r_{i-1} and for the ingoing ones $\boldsymbol{I}^-$ at r_i. The resulting equation can be written

$$\begin{bmatrix} \boldsymbol{I}^+(r_{i-1}) \\ \boldsymbol{I}^-(r_i) \end{bmatrix} = \begin{bmatrix} \boldsymbol{t}^+ & \boldsymbol{r}^+ \\ \boldsymbol{r}^- & \boldsymbol{t}^- \end{bmatrix} \begin{bmatrix} \boldsymbol{I}^+(r_i) \\ \boldsymbol{I}^-(r_{i-1}) \end{bmatrix} + \begin{bmatrix} \boldsymbol{S}^+ \\ \boldsymbol{S}^- \end{bmatrix} . \tag{A3}$$

The t and r matrices can be interpreted as operators describing the transmission and reflection of photons. The matrix functions $S^{\pm}$ describe the effects of photon sources.

For the evaluation of equation (A2), we calculate the matrix exponential function by diagonalization. However, it is then immediately seen that, because a ray and its counterpart in the opposite direction are weakened in the same way, both positive and negative eigenvalues occur. Since the eigenvalues are of the order $1/\mu$ and they have to be multiplied by the optical depth the corresponding exponential terms may become so large that a numerical evaluation is not possible. However, as was shown by Schmidt & Wehrse (1987) these positive eigenvalues can be eliminated analytically and then the terms in equation (A3) can be written in a form suitable for numerical calculations.

When the operators have been evaluated for all shells and it is realized that the intensities leaving one shell are identical with those entering the next shell, all intensities are derived by the combined solution of equation (A3) for $i = 1 \ldots N_s$, i.e., by the solution of a (large) linear system with bandstructure which formally can be written

$$\tilde{\boldsymbol{I}}_l = \boldsymbol{\Omega}_l \tilde{\boldsymbol{B}}_l \,. \tag{A4}$$

Now a Newton-Raphson scheme can easily be set up to fulfill the energy equation since the Jacobian is given by

$$\frac{\partial \tilde{\boldsymbol{F}}}{\partial \tilde{\boldsymbol{T}}} = \sum_l \frac{\partial \tilde{\boldsymbol{F}}_l}{\partial \tilde{\boldsymbol{T}}} = \sum_l \frac{\partial \boldsymbol{\Omega}_l}{\partial \tilde{\boldsymbol{T}}} \tilde{\boldsymbol{B}} = \boldsymbol{\Omega}_l \frac{\partial \tilde{\boldsymbol{B}}_l}{\partial \tilde{\boldsymbol{T}}} \tag{A5}$$

and the temperature corrections can be written

$$\Delta \tilde{\boldsymbol{T}} = -\left(\frac{\partial \tilde{\boldsymbol{F}}}{\partial \tilde{\boldsymbol{T}}}\right)^{-1} \Delta \tilde{\boldsymbol{F}} \,. \tag{A6}$$

REFERENCES

Abramowitz, M., & Stegun, I. A. 1965, Handbook of Mathematical Functions (New York: Dover)
Andreä, J., Drechsel, H., Snijders, M. A. J., & Cassatella, A. 1991, A&A, 244, 111
Auer, L., & Mihalas, D. 1969, ApJ, 158, 641
Austin, S., Starrfield, S., Saizar, P., Shore, S. N., & Sonneborn, G. 1990, in Evolution in Astrophysics: *IUE* Astronomy in the Era of New Space Missions, ed. E. Rolfe (Noordwijk: ESA SP 310), 367
Austin, S., Starrfield, S., Saizar, P., Sparks, W. M., Sonneborn, G., Wagner, R. M., & Wade, R. 1992, in preparation
Baschek, B., Scholz, M., & Wehrse, R. 1991, A&A, 246, 374
Bath, G. T., & Shaviv, G. 1976, MNRAS, 197, 305
Bode, M. F., & Evans, A. 1989, Classical Novae (New York: Wiley)
Cassatella, A., & Gonzalez-Riestra, R. 1990, in Physics of Classical Novae, ed. A. Cassatella & R. Viotti (Heidelberg: Springer), 115
Cassatella, A., & Viotti, R. 1990, Physics of Classical Novae (Heidelberg: Springer)
Eastman, R. G., & Kirshner, R. P. 1989, ApJ, 347, 771
Evans, A. 1990, in Physics of Classical Novae, ed. A. Cassatella & R. Viotti (Heidelberg: Springer), 253
Gehrz, R. D. 1988, ARA&A, 26, 377
———. 1990, in Physics of Classical Novae, ed. A. Cassatella & R. Viotti (Heidelberg: Springer), 138
Gierens, K. M., Traving, G., & Wehrse, R. 1987, J. Quant. Spectros. Rad. Transf., 37, 361
Harkness, R. P. 1983, MNRAS, 204, 45
Hauschildt, P. H. 1991, Ph.D. thesis, Universität Heidelberg
———. 1992, J. Quant. Spectros. Rad. Transf., in press
Hauschildt, P. H., Best, M., & Wehrse, R. 1991, A&A, 247, L21
Hauschildt, P. H., Shaviv, G., & Wehrse, R. 1989, A&A, 210, 262
Hauschildt, P. H., & Wehrse, R. 1991, J. Quant. Spectros. Rad. Transf., 46, 81
Hjellming, R. M. 1990, in Physics of Classical Novae, ed. A. Cassatella & R. Viotti (Heidelberg: Springer), 169
Johnson, L. C. 1972, ApJ, 174, 227
Krautter, J., Beuermann, K., Leitherer, C., Oliva, E., Moorwood, A. F. M., Deul, E., Wargau, W., Klare, G., Kohoutek, L., van Paradijs, J., & Wolf, B. 1984, A&A, 137, 307
Kurucz, R. L. 1988, private communication
Kurucz, R. L., & Peytremann, E. 1975, Smithsonian Astrophys. Obs. Spec. Rept., No. 362
Mathisen, R. 1984, Univ. of Oslo Publ. Ser., No. 1
Mihalas, D. 1978, Stellar Atmospheres (San Francisco: Freeman)
Mihalas, D., & Weibel-Mihalas, B. 1984, Foundations of Radiation Hydrodynamics (Oxford Univ. Press)
Ögelman, H. B. 1990, in Physics of Classical Novae, ed. A. Cassatella & R. Viotti (Heidelberg: Springer), 148
Olson, G. L., & Kunasz, P. B. 1987, J. Quant. Spectros. Rad. Transf., 38, 325
Saizar, P., Starrfield, S., Ferland, G. J., Wagner, R. M., Truran, J. W., Kenyon, S. J., Sparks, W. M., Williams, R. E., & Stryker, L. L. 1991, ApJ, 367, 310
Saizar, P., et al. 1992, ApJ, submitted
Schmidt, M., & Wehrse, R. 1987, in Numerical Radiative Transfer, ed. W. Kalkofen (Cambridge: Cambridge Univ. Press), 341
Shara, M. M. 1989, PASP, 101, 5
Shine, R. A. 1973, Ph.D. thesis, Univ. Colorado
Shine, R. A., & Linsky, J. L. 1974, Sol. Phys., 39, 49
Shore, S. N., Sonneborn, G., Starrfield, S., Hamuy, M., Williams, R. E., Cassatella, A., & Drechsel, H. 1991, ApJ, 370, 193
Shore, S. N., et al. 1992, in preparation
Snijders, M. A. J., Batt, T. J., Roche, P. F., Seaton, M. J., Morton, D. C., Spoelstra, T. A. T., & Blades, J. C. 1987, MNRAS, 228, 329
Sonneborn, G., Shore, S. N., & Starrfield, S. 1990, in Evolution in Astrophysics: *IUE* in the Era of New Space Missions, ed. E. Rolfe (Noordwijk: ESA SP-310), 439
Sparks, W. M., Starrfield, S., Truran, J. W., & Kutter, G. S. 1988, in Diagnostics of Stellar Evolution and Atmospheric Phenomena in Stellar Explosions, ed. K. Nomoto (Heidelberg: Springer), 234
Starrfield, S. 1989, in Classical Novae, ed. M. F. Bode & A. Evans (New York: Wiley), 39
———. 1990, in Physics of Classical Novae, ed. A. Cassatella & R. Viotti (Heidelberg: Springer), 127
———. 1992, in Binary Stars, ed. Y. Kondo & J. Sahade (Utrecht: Kluwer), in press
Starrfield, S., & Snijders, M. A. J. 1987, in Scientific Accomplishments of the *IUE* Satellite, ed. Y. Kondo (Dordrecht: Reidel), 377
Stenholm, L. G., Störzer, H., & Wehrse, R. 1989, J. Quant. Spectros. Rad. Transf., 45, 47
Stryker, L. L., et al. 1988, in A Decade of UV Astronomy with the *IUE* Satellite, ed. E. Rolfe (Nordwijk: ESA SP-281), Vol. 1, 149
Suzuki, M. 1986, IAU Circ., No. 4281
Truran, J. W., & Livio, M. 1986, ApJ, 308, 721
Williams, R. E., Ney, E. P., Sparks, W. M., Starrfield, S., & Truran, J. W. 1985, MNRAS, 212, 753
Williams, R. E., Sparks, W. M., Gallagher, J. S., Ney, E. P., Starrfield, S., & Truran, J. W. 1981, ApJ, 251, 221